

Accepted Manuscript

Metabolic Functions of Gut Microbes Associate With Efficacy of Tumor Necrosis Factor Antagonists in Patients with Inflammatory Bowel Diseases

Konrad Aden, Ateequr Rehman, Silvio Waschina, Wei-Hung Pan, Alesia Walker, Marianna Lucio, Alejandro Mena Nunez, Richa Bharti, Johannes Zimmerman, Johannes Bethge, Berenice Schulte, Dominik Schulte, Andre Franke, Susanna Nikolaus, Johann Oltmann Schroeder, Doris Vandeputte, Jeroen Raes, Silke Szymczak, Georg H. Waetzig, Rainald Zeuner, Philippe Schmitt-Kopplin, Christoph Kaleta, Stefan Schreiber, Philip Rosenstiel

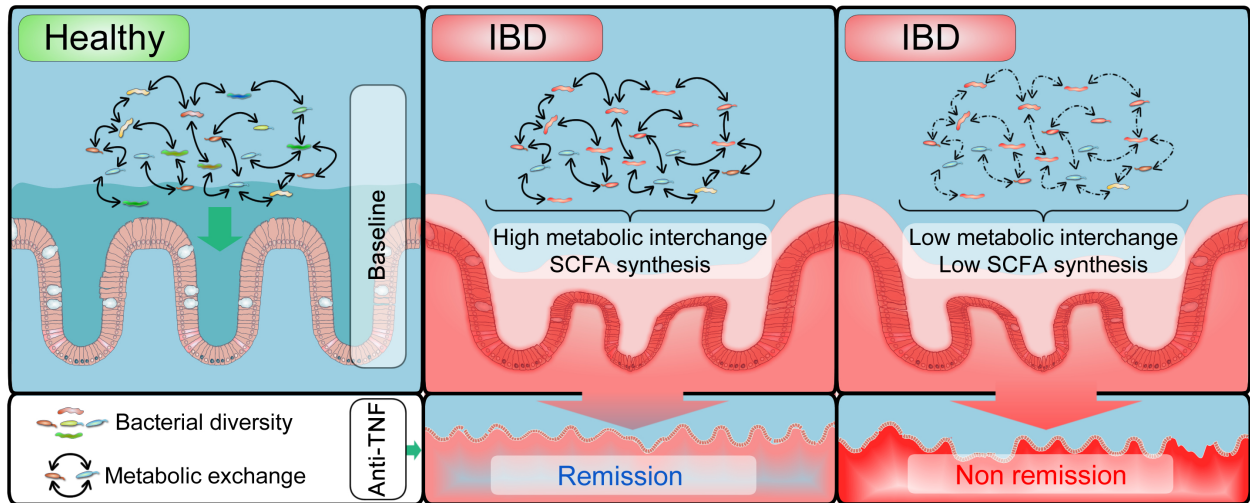
PII: S0016-5085(19)41118-9
DOI: <https://doi.org/10.1053/j.gastro.2019.07.025>
Reference: YGAST 62776

To appear in: *Gastroenterology*
Accepted Date: 4 July 2019

Please cite this article as: Aden K, Rehman A, Waschina S, Pan W-H, Walker A, Lucio M, Nunez AM, Bharti R, Zimmerman J, Bethge J, Schulte B, Schulte D, Franke A, Nikolaus S, Schroeder JO, Vandeputte D, Raes J, Szymczak S, Waetzig GH, Zeuner R, Schmitt-Kopplin P, Kaleta C, Schreiber S, Rosenstiel P, Metabolic Functions of Gut Microbes Associate With Efficacy of Tumor Necrosis Factor Antagonists in Patients with Inflammatory Bowel Diseases, *Gastroenterology* (2019), doi: <https://doi.org/10.1053/j.gastro.2019.07.025>.

This is a PDF file of an unedited manuscript that has been accepted for publication. As a service to our customers we are providing this early version of the manuscript. The manuscript will undergo copyediting, typesetting, and review of the resulting proof before it is published in its final form. Please note that during the production process errors may be discovered which could affect the content, and all legal disclaimers that apply to the journal pertain.





Metabolic Functions of Gut Microbes Associate With Efficacy of Tumor Necrosis Factor Antagonists in Patients with Inflammatory Bowel Diseases

Authors

Konrad Aden^{1,2*}, Ateequr Rehman^{1*}, Silvio Waschina^{3*}, Wei-Hung Pan¹, Alesia Walker⁴, Marianna Lucio⁴, Alejandro Mena Nunez¹, Richa Bharti¹, Johannes Zimmerman³, Johannes Bethge², Berenice Schulte², Dominik Schulte², Andre Franke¹, Susanna Nikolaus², Johann Oltmann Schroeder², Doris Vandeputte⁵, Jeroen Raes⁵, Silke Szymczak⁶, Georg H. Waetzig⁷, Rainald Zeuner², Philippe Schmitt-Kopplin⁴, Christoph Kaleta³⁺, Stefan Schreiber^{1,2+}, and Philip Rosenstiel¹⁺

Affiliation

1 Institute of Clinical Molecular Biology, Christian-Albrechts-University and University Hospital Schleswig-Holstein, Campus Kiel, 24105 Kiel, Germany

2 Department of Internal Medicine I, Christian-Albrechts-University and University Hospital Schleswig-Holstein, Campus Kiel, 24105 Kiel, Germany

3 Institute for Experimental Medicine, Christian-Albrechts-University and University Hospital Schleswig-Holstein, Campus Kiel, 24105 Kiel, Germany

4 Research Unit Analytical BioGeoChemistry, Helmholtz Zentrum München, German Research Centre for Environmental Health (GmbH), Neuherberg, Germany

5 VIB-KU Leuven Center for Microbiology, Campus Gasthuisberg, 3000 LEUVEN, Belgium

6 Institute of Medical Informatics and Statistics, University of Kiel, Germany

7 CONARIS Research Institute AG, Kiel, Germany

*These authors contributed equally

+ shared senior authorship

Grant Support: This work was funded by the BMBF-initiative E:med sysINFLAME, the Clusters of Excellence Inflammation at Interfaces and Precision Medicine in Chronic

Inflammation (ExC 306 and 2167), the EU H2020 SYSCID program under the grant agreement No 733100 and the DFG (SCHR 512/14-1).

Abbreviations: CD, Crohn's disease; UC, Ulcerative colitis; RA, Rheumatoid arthritis; CID, Chronic inflammatory disease

Correspondence: Philip Rosenstiel, MD; Institute of Clinical Molecular Biology, University Hospital Schleswig-Holstein, Campus Kiel; Rosalind-Franklin-Straße 12, D-24105 Kiel, Germany, Phone: +49 (431) 500-15111, Fax: +49 (431) 500-12070; E-mail: p.rosenstiel@mucosa.de or Stefan Schreiber; Department of Internal Medicine I, University Hospital Schleswig-Holstein, Campus Kiel; Rosalind-Franklin-Straße 12, D-24105 Kiel, Germany, Phone: +49 (431) 500-22201, Fax: +49 (431) 500-15104, s.schreiber@mucosa.de

Disclosure: Konrad Aden has received funding from Pfizer to execute parts of this study. The grant did not affect study design at any time point. All other authors have nothing to disclose.

Author contribution: KA and PR designed study; KA, SN, JOS, RZ and JB collected biosamples and performed clinical scoring; AR, WHP, RB, SW and JZ performed sequencing and analysis; SW, JZ, CK, DV and JR performed *in silico* analysis of bacterial community assembly and metabolism; AW and PSK performed metabolomics; CK, JR, SSz, GHW and AF performed critical revision of the manuscript for important intellectual content; KA, AR, SW, JZ, CK, SS and PR wrote the manuscript.

Abstract

Background & Aims: Altered interactions between the mucosal immune system and intestinal microbiota contribute to pathogenesis of inflammatory bowel diseases (IBD). It is not clear how inhibitors of cytokines, such as antagonists of tumor necrosis factor (anti-TNF), affect the intestinal microbiome. We investigated the effects of anti-TNF agents on gut microbe community structure and function in a longitudinal 2-step study of patients with IBD. We correlated our findings with outcomes of treatment and investigated patterns of metabolites in fecal samples before and after anti-TNF therapy.

Methods: We performed a prospective study of 2 cohorts of patients in Germany; the discovery cohort comprised 12 patients with IBD, 17 patients with rheumatic disease, and 19 healthy individuals (controls); fecal samples were collected at baseline and 2, 6, and 30 weeks after induction of anti-TNF therapy. The validation cohort comprised 23 patients with IBD treated with anti-TNF or vedolizumab (anti- $\alpha 4\beta 7$ integrin) and 99 healthy controls; fecal samples were collected at baseline and at weeks 2, 6, and 14. Fecal microbiota were analyzed by V3–V4 16S rRNA gene amplicon sequencing. Clinical response and remission were determined by clinical disease activity scores. Metabolic network reconstruction and associated fecal metabolite level inference was performed *in silico* using the AGORA resource. Metabolomic analyses of fecal samples from a subset of patients were performed to validate metabolites associated with treatment outcomes.

Results: Anti-TNF therapy shifted the diversity of fecal microbiota in patients with IBD, but not with rheumatic disease, toward that of controls. Across timepoints, diversity indices did not vary significantly between patients with IBD who did or did not achieve clinical remission after therapy. In contrast, *in silico* modeling of metabolic interactions between gut microbes found metabolite exchange to be significantly reduced at baseline in fecal samples from patients with IBD and to be associated with later clinical remission. Predicted levels of butyrate and substrates involved in butyrate synthesis (ethanol or acetaldehyde) were significantly associated with clinical remission following anti-TNF therapy, verified by fecal metabolomic analyses.

Conclusions: Metabolic network reconstruction and assessment of metabolic profiles of fecal samples might be used to identify patients with IBD likely to achieve clinical remission following anti-TNF therapy and increase our understanding of the heterogeneity of IBD.

KEY WORDS: Crohn's disease, ulcerative colitis, inflammation, short-chain fatty acid

Introduction

Inflammatory bowel disease (IBD) with its main entities Crohn's disease (CD) and ulcerative colitis (UC) can be considered an archetypal disease entity of a larger, heterogeneous group of chronic inflammatory diseases (CIDs), characterized by a dysbalanced immune system, leading to excessive pro-inflammatory cytokine production and destructive local inflammation^{1, 2}. CIDs affect different organs through their primary manifestation but are characterized by common systemic immune perturbations. The underlying etiology comprises a polygenic susceptibility

with more than 200 risk variants and loci identified for IBD until today³⁻⁵ and many of these are shared between the different CID entities. Shared disease genes are preferentially involved in the regulation of innate and adaptive immune responses and are thought to affect the homeostasis of host-microbiota interactions^{6, 7}. Intestinal dysbiosis has been detected across CIDs.^{8, 9} While dysbiosis in IBD^{10, 11, 12, 13} is likely influenced by immune dysregulation and destruction of the epithelial interface by local inflammation, the etiology of dysbiosis seen in other CIDs without overt inflammation in the gut is still vague and comprises shifts of specific bacterial taxonomical groups and enrichment of potentially harmful taxa, e.g. *Eggerthella lenta* in rheumatoid arthritis (RA).^{14, 15} Despite an immanent need to understand the underlying mechanism of dysbiosis, a systematic comparison of gut microbial communities in intestinal vs. non-intestinal driven inflammatory disease is missing so far. Blockade of TNF has evolved as a therapeutic principle that is effective across different CIDs.^{16, 17} Although the use of anti-TNF antibodies is a mainstay for the therapy in CID, the development of antibodies directed against other pro-inflammatory cytokines (IL-6, IL-1 β) and lately also the exploitation of other principles, e.g. blockade of integrin-mediated immune cell trafficking in IBD,¹⁸ has led to an increased complexity in the treatment of these CID entities.

To what extent targeted therapies are able to interfere with altered gut microbial community structures and metabolic function is unknown. Likewise, whereas it was shown in cancer therapy that efficacy of targeted therapies, such as immunotherapy as well as classical chemotherapy, is critically modulated by gut microbial community composition,^{19, 20} it is unknown whether gut microbiota and related metabolic properties are associated with therapeutic outcome. Here, we investigated the role of anti-TNF therapy on longitudinal dynamics of gut microbial composition and metabolic function in a two-tiered approach. First, we investigated the influence of anti-TNF

on gut microbial diversity by 16S rRNA phylogenetic profiling and ecosystem-scale metabolic modeling in patients with IBD or rheumatic diseases. We show that inferred microbial metabolic interactions are associated with response to anti-TNF therapy in patients with IBD. In a second step, we validated our findings in an independent IBD cohort and found that microbial metabolite interactions are able to discriminate between anti-TNF remitter and non-remitters. Using in-silico prediction of metabolite exchange and stool metabolomics, we show that, among other principles, butyrate levels are significantly altered between patients achieving remission vs. non-remitting patients. We thereby demonstrate that i) 16S rRNA based functional prediction of metabolic cooperativity might serve as a novel approach for predicting clinical response to TNF antagonists in patients with IBD and ii) identify the SCFA butyrate as a clinical marker for therapeutic efficacy in IBD.

MATERIALS AND METHODS

Patient recruitment and study design

Human study subjects were recruited at the outpatient clinic of the University Hospital Schleswig-Holstein, Campus Kiel, to obtain fecal samples. Treatment decisions were made due to clinical requirements after discussion at the interdisciplinary inflammatory medicine board of the hospital. The design of the prospective studies had no influence on treatment or other clinical actions. Patients were naïve to biological treatment or had at least paused prior biologic therapy for more than 12 weeks. The study was approved by the ethics committee of the Christian-Albrechts-University of Kiel (A 124/14 and AZ 156/03-2/13) and subjects provided written informed consent.

For the discovery cohort (cohort #1), patients were recruited from two major patient groups, (i) 12 patients with intestinal inflammation (i.e. IBD, UC (n=4), CD (n=8)) or (ii) with non-IBD rheumatic diseases (i.e. seropositive rheumatoid arthritis (n=10), seronegative rheumatoid arthritis (n=2), ankylosing spondylitis (n=5)), which are collectively termed rheumatic diseases (n=17) hereafter. Patients were asked to collect morning feces before (24 h) and at designated time points (2, 6 and 30 weeks) after anti-TNF therapy initiation. Fecal samples were collected using feces collection tubes with prefilled DNA stabilizer (Stratec, Birkenfeld, Germany) and stored at -80°C until further use. Anti-TNF agents comprised infliximab, certolizumab pegol, adalimumab, and etanercept. Single time point samples from a group of 19 healthy, untreated subjects were included at the same time and using identical sampling procedures were included into the study as controls. For the validation cohort (cohort #2), a total of 23 biologics-naïve patients with IBD (CD=10, UC=13) were recruited, who received first-time anti-TNF (infliximab, n=10) or anti- $\alpha 4\beta 7$ integrin antibody (vedolizumab, n=13) therapy. Patients were investigated within a 24-hour time frame before initiation of treatment and at weeks 2, 6, and 14 after initiation of treatment including collection of morning feces. Single time-point fecal 16S rRNA gene microbial profiles from a cross sectional cohort of healthy individuals (n=99) sampled in the time frame of the study served as a reference map to assess the directionality of microbial changes after anti-TNF therapy initiation for cohort #2. Overview of patient characteristics are detailed in **Supplementary Table 1**. Overview of clinical efficacy data for the two cohorts are shown in **Supplementary Tables 2 and 3**, respectively. A detailed overview about cohort composition and molecular analyses is given in **Supplementary Figure 1**.

Patient assessment

All patients were scheduled for biologic therapy for medical reason and received drug at least until week 22. Clinical disease indices were assessed at baseline and at weeks 2, 6, 14 and 30 after therapy initiation using clinical disease scores (Disease Activity Score 28 for RA (DAS28), Bath Ankylosing Spondylitis Disease Activity Index (BASDAI), Harvey-Bradshaw Index for CD (HBI) or Mayo score for UC).²¹ In RA, clinical response was defined as a reduction of the DAS28 score by more than 1.2 points, whereas clinical remission was defined as a DAS28 <2.6. For ankylosing spondylitis, the BASDAI clinical response was defined as a reduction of 50% (BASDAI50) at week 6, whereas clinical remission was defined as a BASDAI <4. Responders in the HBI for CD were defined by a decrease of ≥ 2 points in HBI while non-responders showed a decrease of < 2 points or an increase in HBI. CD patients with an HBI of ≤ 4 were considered to be in remission, those with ≥ 5 to have active disease. In patients with UC, a decrease of the partial Mayo score of ≥ 2 points and $\geq 30\%$ with either a decrease of rectal bleeding ≥ 1 or with rectal bleeding ≤ 1 were defined as responder. Patients with a partial Mayo Score of ≤ 2 (bleeding 0) were considered to be in remission, those with ≥ 3 to have active disease. Histopathological scoring of biopsies was performed by standard clinical procedures in a blinded fashion by a trained pathologist, and the overall grade of inflammation was grouped according to normal (0), mild (1), moderate (2) or severe inflammation (3), and the respective values were used for pathology score calculation.

Statistical analyses

Phylotype abundances were subsampled to the lowest number of sequences within the analysed sample and relative abundances were \log_{10} -normalized. Principal coordinate analysis (PcoA) was performed on abundance (Bray-Curtis) and presence/absence (Jacquard) based distance matrices.

One-way permutational multivariate analysis of variance (PERMANOVA) was performed to test the statistical significance of microbial community differences in healthy subjects and patients with IBD or rheumatic diseases. Both PCoA and PERMANOVA were performed in PAST software and principle coordinates were visualized in the vegan package v.2.0-10 in R software V 3.0.3 (<https://cran.r-project.org/web/packages/vegan/index.html>). We employed the Θ_{YC} (Yue-Clayton) similarity index²² to measure the shift of microbiota before and after initiation of treatments (within and between disease groups) as well as directionality in reference to healthy subject microbiota. This similarity index is based on the species abundance of shared as well as non-shared species applying even weighting to all species in communities. The non-parametric Mann-Whitney U test was employed to test the significance of diversity/distance differences between healthy subjects and patients (IBD/rheumatic diseases) at different time points. The non-parametric Wilcoxon matched-pairs signed rank test was used to observe the significance of changes before and after therapy initiation within a disease group. Indicator species analysis²³ was performed to identify indicator bacterial phylotypes between healthy control group and patients (IBD and rheumatic diseases) before and 30 weeks after therapy initiation. This approach takes relative abundance and relative frequency of occurrence in two sets of samples²⁴ into account.

Microbial community modelling

We used reconstructed metabolic models of 773 human gut bacterial species²⁵ (AGORA resource) to predict metabolic potential and biochemical interactions between bacterial species. We extensively refined the originally published models to remove erroneous futile cycles that occurred in community simulations and often caused unreasonably high exchange fluxes

between bacteria (see **Supplementary Table 6** for details). By mapping 16S rRNA sequences to the corresponding models contained in AGORA and combining them to a community-level metabolic model, we derived patient-specific models of the respective microbial community. Using these models, we inferred ecological relationships (mutualism, competition, antagonism) and potential metabolite exchange interactions with the host. Please refer to the Supplementary Materials and Methods for a more detailed description.

RESULTS:

Chronic inflammatory diseases are characterized by intestinal dysbiosis

We investigated microbiota community structures of IBD, healthy controls (HC) and patients with rheumatic diseases (seropositive/seronegative rheumatoid arthritis or ankylosing spondylitis) at baseline. This discovery cohort comprised longitudinal fecal samples of a total of 29 patients (IBD=12, rheumatic diseases=17) before and after anti-TNF therapy initiation and single time point fecal samples from HC (n=19) (**Tables S1 and S2**). 16S rRNA gene sequencing of all samples (including baseline and post therapeutic intervention) resulted in the identification of 388 phylotypes (**Table S4, Supplementary Materials and Methods**). As all statistical algorithms assessing α -diversity have inherent strengths and weaknesses, we used a set of α -diversity indices including (i) observed and (ii) estimated (Chao I) richness, (iii) evenness of species considering abundance (non-parametric Shannon) and (iv) phylogenetic distance (phylodiversity score). Comparing all groups, baseline microbial communities between healthy controls and the rheumatic disease or IBD groups, respectively, were significantly different, as shown by non-parametric Kruskal-Wallis test. To interrogate pairwise baseline differences of microbial α -diversity between specific groups, we used the Mann-Whitney U test, which – for the pair IBD vs. HC – showed significantly reduced α -diversity index values for i)

observed ($p = 0.024$; **Figure 1A**) and ii) estimated (Chao I) richness ($p = 0.019$; **Figure 1B**), iii) NP Shannon index of diversity ($p = 0.0001$; **Figure 1C**) and iv) phylogenetic diversity ($p = 0.017$; **Figure 1D**). Patients with rheumatic diseases also had reduced bacterial diversity compared to HC, but the index levels were only significant for the NP Shannon diversity index (**Figure 1C**). Principal coordinate analysis (PcoA) on membership- (Jaccard) and abundance-based (Bray-Curtis) β -diversity distance matrices demonstrate that the first two coordinates were able to separate samples for a health/disease descriptor status. PERMANOVA test on Jaccard (**Figure 1E**) distances showed a significantly distinct microbial composition between IBD, rheumatic diseases and HC. Similarly, abundance (Bray-Curtis)-based analysis revealed significant differences in patients with IBD and rheumatic diseases compared to HC, but the differences were not significant between rheumatic diseases and IBD communities (**Figure 1F**). These observations confirm earlier findings¹¹ showing that the baseline intestinal microbial communities of patients with IBD are characterized by a reduced number of species and diminished richness and evenness (α -diversity) as well as altered community composition and structure (β -diversity). In contrast, intestinal microbiota from patients with rheumatic diseases only display shifts in community structure (β -diversity) compared to HC, indicating a disease effect on the gut microbiota even in the absence of overt intestinal inflammation.

Effects of anti-TNF treatment on microbial diversity in IBD and rheumatic diseases are reflected on the β - but not α -diversity level

To analyze the effect of anti-TNF treatment on intestinal microbiota in IBD ($n=12$) and rheumatic diseases ($n=17$) independently, we assessed α -diversity indices before and 2, 6 and 30 weeks after first-time anti-TNF therapy induction and used the samples of the HC group as

reference point. The observed and estimated species richness and phylodiversity in patients with IBD increased after the beginning of therapeutic intervention and reached statistical significance at week 30 compared to baseline. This shift was directed towards the controls, and the distance between diversities of treatment naïve IBD fecal samples and healthy controls became non-significant after 30 weeks of therapy (**Figures 2A, 2B and 2D**). Similar differences were not observed for the NP Shannon diversity index (**Figure 2C**). In contrast, restoration of bacterial diversities was not evident in patients with rheumatic diseases (**Figure 2E-H**). Interestingly, we failed to identify a discrimination between remitting and non-remitting patients based on α -diversity restorations (**Figure S2**), which could also be due to limited sample size. We next investigated β -diversity indices to measure longitudinal community composition changes before and after therapy initiation. We assessed the inter-individual dissimilarity using Yue and Clayton distance matrix, which considers not only membership overlap, but also species abundance between communities.²² Pairwise comparison of distances between samples at baseline and during treatment (2, 6 and 30 weeks) showed increased inter-individual dissimilarity among anti-TNF-treated IBD patients (**Supplementary Figure 3A**). This indicates that anti-TNF treatment induces an increase of heterogeneity of the intestinal microbiota between patients with IBD. In contrast to IBD, anti-TNF treatment in patients with rheumatic diseases during treatment was associated with an overall decrease of dissimilarity (week 30 vs. pre-treatment) of the microbiota (**Supplementary Figure 3B**). This indicates an overall constriction of microbial β -diversity, i.e. a gain of similarity, between patients with rheumatic diseases. To understand the directionality of the observed changes, we compared dissimilarity between healthy subjects and disease groups (IBD, rheumatic diseases) before and during therapeutic intervention and observed that anti-TNF treatment shifted the microbial communities of both patient groups towards healthy subjects,

indicating a subtle corrective effect of anti-TNF treatment on microbial dysbiosis of both disease entities, IBD and rheumatic diseases (**Supplementary Figures 3C, 3D**). Again, a discrimination between clinical remission and non-remission was not observable (data not shown).

Individual phylotype alterations after anti-TNF treatment

We next determined indicator bacterial phylotypes that were significantly different between healthy control (HC) and anti-TNF treated patients with IBD or rheumatic diseases at baseline and asked whether these taxa would alter their abundance upon anti-TNF treatment (week 30). In IBD, we identified 14 indicator phylotypes that were significantly different between HC from untreated IBD (**Supplementary Table 5**). Upon anti-TNF treatment, all 14 identified phylotypes lost the indicator species status, suggesting that these phylotypes are normalized upon anti-TNF treatment (**Figure 3A**). In IBD, *Coprococcus* (indicator value, 84.37; $p = 0.003$) and *Roseburia inulinivorans* (indicator value, 79.25; $p = 0.031$) were the top indicator phylotypes at baseline (based on p-value, compared to HC). Both indicator phylotypes displayed reduced abundance compared to healthy subjects at week 0 and increased their abundance over the time course of treatment, leading to loss of significance between HC and IBD at week 30 (**Figure 3B, Supplementary Table 5**). In patients with rheumatic diseases, we identified 5 indicator phylotypes, which – by abundance – were significantly different between baseline and HC and lost the indicator status after anti-TNF treatment at week 30 (**Supplementary Figure 4A, Supplementary Table 6**). Of those 5 indicator taxa, the abundance of the top indicator phylotypes (week 0 compared to HC, based on p-value) *Erysipelotrichaceae* (indicator value, 81.33; $p = 0.009$) and *Dorea* (indicator value, 68.81; $p = 0.042$) increased significantly to become non-indicators in post-treatment samples at week 30 (**Supplementary Figure 4B**).

Strikingly, none of these identified taxa were significantly associated with therapeutic outcome of anti-TNF treatment (remission/non-remission). We therefore hypothesized that such outcome-associated shifts might be better visible in the inferred metabolic pathways and functional properties of the microbiota, which are known to display a greater interindividual consistency compared to the highly variable abundance of individual taxa.²⁶

Stabilizing ecological interactions are less frequent in IBD and rheumatic diseases

As diversity measurements and individual taxa identification in our exploratory cohort were not able to predict therapy outcome in IBD, we next used *in silico* metabolic modeling from 16S rRNA sequencing data to infer metabolic interactions within the luminal microbiota and associated fecal metabolite levels. We hypothesized that metabolic functions rather than taxonomical composition might affect response to TNF antagonists. For this purpose, we employed the recently published AGORA resource, a comprehensive assembly of metagenomics data from 773 human gut bacterial species, designed to predict metabolic interactions among microbial communities based on 16s rRNA data.²⁵ We categorized ecological relationships between two different bacterial organisms into mutualistic interactions, antagonistic interactions, and resource competition, depending on the benefit that the individual partners obtained from the predicted interactions. While mutualistic and antagonistic interactions can increase community dynamics,^{27, 28} interspecific resource competition can reduce community stability.²⁷ Interestingly, the predicted frequencies for mutualistic pairwise interactions did not show significant differences between patients with IBD or rheumatic diseases compared to healthy controls. However, we found that in IBD, and to a lesser degree in rheumatic diseases, the predicted frequency of antagonistic interactions was significantly reduced at the beginning of the therapy

and partially restored towards the end of the treatment (**Figure 4A**). Vice versa, we observed an enhanced interspecific resource competition of gut bacteria in both inflammatory diseases, indicating a reduced stability of microbial communities.

Metabolic cross-feeding is impaired in patients with IBD and rheumatic diseases and associated with lack of clinical efficacy of anti-TNF therapy

To evaluate whether anti-TNF treatment also affects the rates (or fluxes) of metabolite exchange between organisms (referred to as '*metabolic interchange*'), we used metabolic network modeling to predict the exchange of metabolites between bacterial community members in the individual samples using *in silico* microbial community models (for details see Supplementary Materials and Methods). The simulation results indicated that non-remitting patients with IBD or rheumatic diseases, compared to HC, displayed a baseline reduction of total metabolic interchange, which also remained below the levels of HC after 30 weeks of anti-TNF treatment (**Figure 4B**). This was in contrast to patients achieving clinical remission, who did not display a reduction of the predicted metabolic interchange (**Figure 4B**) compared to HC patients. These data point towards different microbial metabolic signatures that might affect therapeutic efficacy and contribute to clinical remission. In summary, the *in-silico* modeling of the gastrointestinal bacterial metabolism indicated a strong disruption of ecosystem functioning within IBD and rheumatic diseases gut microbiomes, which was partly restored upon anti-TNF therapy.

Anti-TNF therapy restores disrupted gut microbial community metabolism in IBD

We next aimed to validate our central hypothesis that impaired metabolic cross-feeding is associated with clinical outcome of anti-TNF therapy in IBD using a second, independent

longitudinal IBD cohort (see **Supplementary Table 7**). In this context, we also aimed to investigate whether these potential effects were attributed to anti-TNF therapy alone or reflected a generalizable effect of successful remission induced by treatment with biologics. We recruited a total of 23 patients (CD=10, UC=13) (Cohort #2), who underwent first-time therapy with either anti-TNF (infliximab; IFX) or anti- $\alpha 4\beta 7$ integrin (vedolizumab) antibodies and collected fecal samples at baseline and at week 2, 6 and 14 after therapy induction (**Supplementary Table 3**). To exclude *a-priori* differences on the dietary intake that might influence microbial community structure, we assessed the dietary intake in a subgroup of patients (n=7 patients, anti-TNF treatment; n=3 remitting, n=4 non-remitting) using the validated Potsdam Dietary Questionnaire²⁹ and were not able to observe significant differences in the intake of carbohydrates, fibers, protein or fat between patients achieving remission or non-remitting patients (data not shown). However, a thorough assessment is needed to fully understand effects of dietary intake on the predicted metabolic properties of the gut microbiota. We performed metabolic cross-feeding analysis on the 16S data sets from the longitudinal fecal samples of either anti-TNF- or anti- $\alpha 4\beta 7$ -integrin-treated patients with IBD and specifically aimed to validate our previous findings from cohort #1, namely that *in silico* prediction of metabolic and ecological interactions associated with clinical efficacy in anti-TNF-treated patients with IBD. Indeed, *in-silico* predictions on bacterial interactions suggested differences in the gastrointestinal microbial ecology depending on the patients' remission status in response to anti-TNF. Only patients that did not achieve clinical remission displayed significantly reduced antagonistic interactions and significantly increased resource competitive interactions, when compared to healthy controls. Both findings were in line with findings from cohort #1, indicating that non-remitting patients with IBD display a disrupted gut microbial ecosystem (**Figure 5A**). Moreover,

the baseline total predicted metabolic interchange (i.e. cross-feeding) was already reduced by 25% \pm 5% (median \pm SE) only in non-remitter IBD-patients compared to healthy controls (**Figure 5B**, top panel; Mann-Whitney U-test, $p = 0.02$), whereas the predicted metabolic interchange of remitter patients with IBD were similar to levels observed for controls (**Figure 5B**, lower panel; Mann-Whitney U-test, $p = 0.48$). To exclude any *a priori* confounding factors that might affect the predicted metabolic interchange, we performed linear regression of gut metabolic interchange with clinical, laboratory and histology-based disease markers at baseline. We were not able to observe significant differences in disease activity parameters (HBI/Mayo at baseline, leukocytes, C-reactive protein, pathology index) that might explain different baseline metabolic interchange between remitting and non-remitting patients (**Supplementary Figure 5**). To assess whether disruption of metabolic interchange was specifically attributed to anti-TNF therapy or displayed a unifying phenomenon of clinical disease state, we investigated the proportion of metabolic interaction pairs between remitters and non-remitters in response to therapy induction with an anti $\alpha 4\beta 7$ -integrin antibody (vedolizumab). Although the sample number of remitters ($n=11$) and non-remitters ($n=2$) was too small to substantiate our findings using a statistically valid method, our observation indicates that disrupted microbial metabolic interchange may also be more pronounced in non-remitters to vedolizumab (**Supplementary Figure 6**).

In-silico meta-analysis of microbial metabolite cross-feeding interactions predicts specific metabolic pathways associated with anti-TNF therapy in IBD

To identify exact metabolite cross-feeding interactions that are disrupted during IBD, we combined the 16S rRNA data from all patients undergoing anti-TNF therapy in cohort #1&2 for an *in-silico* meta-analysis. Principle component analysis on the predicted cross-feeding rates of

374 metabolites revealed neither cohort-derived batch effects nor gender disparities (**Supplementary Figure 7**). From these cross-feeding interactions, we inferred 10 metabolites in non-remitter patients that were less frequently exchanged already at baseline compared to healthy controls. Only three (ethanol, glutamate, glycine) of them were also observable in patients that achieved clinical remission (**Figure 6**, left Venn diagram), suggesting a stronger disruption of the metabolic interaction network in non-remitter patients with IBD. Interestingly, *in-silico* analysis predicted a restoration of some affected metabolites (e.g. butyrate) after anti-TNF therapy (**Figure 6**, right Venn diagram). Overall, non-remitting patients with IBD display a stronger disruption of metabolic interactions (7 metabolites) in response to anti-TNF therapy compared to patients achieving clinical remission (4 metabolites, **Figure 6**). A direct comparison of baseline samples from remitting and non-remitting patients inferred that especially the intercellular exchange of butyrate is significantly reduced by 81% (median) in non-remitter patients compared to patients with IBD that achieved clinical remission (false discovery rate-corrected Mann-Whitney U-test, $P = 0.02$). Overall, these results support the hypothesis that the response to therapy itself is strongly associated to the prevalence of metabolic exchanges in treatment-naïve patients.

Clinical remission in anti-TNF therapy is associated with changes in the stool metabolome

Based on the *in-silico* prediction of gut microbial metabolic cross-feeding interactions, we postulated that anti-TNF therapy might also be associated with changes in fecal metabolites. To test this hypothesis, we investigated the stool metabolome from 9 patients with IBD (CD=3, UC=6, remitting=5, non-remitting=4) at baseline and after 14 weeks of anti-TNF treatment. To define which metabolites were characteristic in baseline, non-remission and remission groups,

we built an orthogonal partial least squares discriminant analysis (OPLS-DA) model (**Figure 7A**). The classification models were highly significant for both datasets. Overall, we observed time-dependent differences between baseline and week 14 and fewer differences due to remission state (**Figure 7A, 7B**). Despite small effects of the treatment, we could find particular metabolites increased at baseline, in remission or in non-remission state (**Figure 7C**). Within the screening set of 50 metabolites (authentic chemical standards), 21 were found in fecal samples and of those 4 metabolites were responsible for the discrimination of the three groups (**Figure 7C**). Whereas the baseline group was discriminated by elevated levels of 3-indolepropionic acid and L-tyrosine, 3-hydroxyphenylacetic acid was increased in the remission group and pyruvic acid in the non-remission group (**Figure 7C**). All other clusters were not identified by an authentic chemical standard and are only putatively annotated on MS1 or MS2 level (summarized in **Supplementary Table 8**). We next investigated whether specific stool metabolites were applicable to delineate clinical remission in anti-TNF treated patients with IBD. Overall, creatinine distinguished untreated (week 0) from anti-TNF treated (week 14) patients, irrespective of remission status. Interestingly and in line with our *in silico* prediction, we found that butyric acid was significantly increased uniquely in the stool metabolome of anti-TNF remission patients. In contrast we found that the metabolite Cluster_1061 annotated as “3-methyl-thiopropionic acid, methyl 2-(methylthio)acetate” (**Figure 7F**) was found to be specifically increased in patients with IBD not achieving remission at week 14.

DISCUSSION

Dysbiosis is defined by altered diversity, composition and structure of the intestinal microbiota but the underlying metabolic principles contributing to dysbiosis remain poorly understood. Most

importantly, it is unknown whether anti-TNF therapy may affect gut microbial composition or function and could thereby contribute to disease control in IBD. In this study, we investigated the interplay of therapeutic anti-TNF inhibition and gut microbiota function in IBD and delineated the effects of organ-specific inflammation (i.e. intestinal vs. non intestinal) on host microbe interaction using patients with rheumatic disease as a non-intestinal inflammatory control cohort. We confirmed that IBD and rheumatic diseases display distinct features of altered microbial community structure and metabolic function in comparison with healthy individuals and thereby confirm previous findings from studies assessing fecal global microbial profiles (α - and β -diversity) in IBD and rheumatic diseases.^{11, 30, 31} While these previously published studies used different techniques and sampling conditions, we present a coherent dataset as a direct side by side comparison of rheumatic diseases and patients with IBD recruited from the same clinical setting. Furthermore, we applied a novel systems biology approach that, for the first time in the context of IBD, allowed us to assess functional consequences of the dysbiotic change in community structure on the level of metabolic interactions within microbial communities. We show that anti-TNF treatment induces restoration of intestinal microbial diversity in IBD, whereas in rheumatic diseases, anti-TNF-associated changes were less pronounced and only transient. We further analyzed anti-TNF-associated shifts of phylotype abundances in IBD and rheumatic diseases by indicator species analysis and identified disease-specific phylotypes that change their abundance over the time course of anti-TNF treatment in either IBD or rheumatic diseases. Notably, we neither identified indicator species that specifically attributed to clinical efficacy of anti-TNF treatment nor did we confirm previously reported associations of increased counts of *Faecalibacterium prausnitzii* at baseline with therapeutic efficacy,³² which both might be attributed to small sample sizes in our study.

It is noteworthy that phylotypes whose abundance changed significantly in patients with IBD towards the direction of healthy subjects (e.g. *Coprococcus* and *Roseburia inulinivorans*) are known short chain fatty acid (SCFA) producers.^{33, 34}

These findings prompted us to interrogate gut metabolic functions using an *in silico*, 16S rRNA gene sequencing-based metabolic cross-feeding analysis. This analysis was conducted to identify metabolic cross-feeding interactions that might contribute to increased butyrate production observed in the case of therapeutic efficacy (remission). Using two independent cohorts of anti-TNF therapy in IBD, we assessed potential metabolic interactions between bacteria within the community using constraint-based modeling. We show that reduction in metabolite cross-feeding interactions and increase of resource competition are present in IBD. Such metabolic interactions are widespread in human intestinal microbiota and are thought to be of high importance for community stability and robustness in a healthy state.³⁵ While mutualistic and antagonistic interactions can stabilize community dynamics and thereby contribute to the maintenance of species diversity,^{27, 28} interspecific resource competition can reduce community stability.²⁷ Moreover, it has been suggested that species co-occurrences in microbial communities are largely driven by metabolic exchanges between cells.³⁶ Indeed, we observed that metabolite exchange interactions could be restored by anti-TNF intervention in IBD. More importantly, we show that, already at baseline level, the total metabolite exchange across bacteria is significantly disrupted in patients with IBD not achieving clinical remission in response to anti-TNF therapy. Lastly, we found that butyrate and substrates involved in butyrate synthesis, such as ethanol or acetaldehyde, were less frequently exchanged among bacterial communities from patients that did not show therapeutic efficacy in response to anti-TNF therapy. Along this line, it has been shown by various studies that disturbances in the microbial networks containing taxa that

typically produce SCFA characterize treatment failure to conventional and biologic therapy.^{37, 38} These findings do not only support the crucial role of SCFA in the disease control of patients with IBD but also underline the feasibility of using 16S *in silico* analysis to predict metabolic pathways that are disrupted in IBD and might affect therapeutic efficacy, which has also been suggested by others.^{39, 40} It is tempting to speculate on the mechanism of action by which biologic therapy is able to restore metabolite exchange interactions in IBD. A robust clinical response to biologic therapy leads to mucosal healing, inducing subsequent changes in host transcriptome architecture.⁴¹ As impaired congruence between host transcriptome and gut microbiome has been described as a distinct feature of IBD,⁴² we assume that re-established congruence upon successful biologic therapy might also affect phylotype-phylotype interactions and metabolite crosstalk among bacteria. However, a further detailed molecular description of changes in the mucosa-associated microbiota and their interaction with host transcriptional changes in the context of anti-TNF treatment is needed to deepen our understanding of the host-microbial interaction and its effect on remission induction.

In summary, we demonstrate that the use of anti-TNF treatment leads to restoration of intestinal microbiome constitution and shifts of disease indicator taxa in human IBD, and we show that specific inferred metabolic interactions between luminal bacteria are associated with therapeutic outcome in IBD. Similar to studies on immune check point inhibitors in cancer, our study clearly suggests functional links between the intestinal microbial ecosystem and therapeutic manipulation by TNF inhibition. Further studies are thus warranted to analyze the exact role of the microbial metabolic interaction network as a potential diagnostic marker or actionable entry point to actively improve therapy control in IBD.

References:

1. Schreiber S, Rosenstiel P, Albrecht M, et al. Genetics of Crohn disease, an archetypal inflammatory barrier disease. *Nat Rev Genet* 2005;6:376-388.
2. McInnes IB, Schett G. Cytokines in the pathogenesis of rheumatoid arthritis. *Nat Rev Immunol* 2007;7:429-442.
3. de Lange KM, Moutsianas L, Lee JC, et al. Genome-wide association study implicates immune activation of multiple integrin genes in inflammatory bowel disease. *Nat Genet* 2017;49:256-261.
4. Franke A, McGovern DPB, Barrett JC, et al. Genome-wide meta-analysis increases to 71 the number of confirmed Crohn's disease susceptibility loci. *Nat Genet* 2010;42:1118-1125.
5. Anderson CA, Boucher G, Lees CW, et al. Meta-analysis identifies 29 additional ulcerative colitis risk loci, increasing the number of confirmed associations to 47. *Nat Genet* 2011;43:246-252.
6. Salmond RJ, Brownlie RJ, Morrison VL, et al. The tyrosine phosphatase PTPN22 discriminates weak self peptides from strong agonist TCR signals. *Nat Immunol* 2014;15:875-883.
7. Spalinger MR, Lang S, Vavricka SR, et al. Protein Tyrosine Phosphatase Non-Receptor Type 22 Modulates NOD2-Induced Cytokine Release and Autophagy. *PLoS ONE* 2013;8:e72384.
8. Hevia A, Milani C, López P, et al. Intestinal Dysbiosis Associated with Systemic Lupus Erythematosus. *mBio* 2014;5.
9. Costello M-E, Ciccia F, Willner D, et al. Brief Report: Intestinal Dysbiosis in Ankylosing Spondylitis. *Arthritis & Rheumatology* 2015;67:686-691.
10. Rehman A, Rausch P, Wang J, et al. Geographical patterns of the standing and active human gut microbiome in health and IBD. *Gut* 2016;65:238-248.
11. Gevers D, Kugathasan S, Denson Lee A, et al. The Treatment-Naive Microbiome in New-Onset Crohn's Disease. *Cell Host & Microbe* 2014;15:382-392.
12. Imhann F, Vich Vila A, Bonder MJ, et al. Interplay of host genetics and gut microbiota underlying the onset and clinical presentation of inflammatory bowel disease. *Gut* 2016.
13. Ott SJ, Musfeldt M, Wenderoth DF, et al. Reduction in diversity of the colonic mucosa associated bacterial microflora in patients with active inflammatory bowel disease. *Gut* 2004;53:685-693.
14. Vaatuovuo J, Munukka E, Korkeamäki M, et al. Fecal Microbiota in Early Rheumatoid Arthritis. *The Journal of Rheumatology* 2008;35:1500-1505.
15. Chen J, Wright K, Davis JM, et al. An expansion of rare lineage intestinal microbes characterizes rheumatoid arthritis. 2016;8:43.
16. Kalliolias GD, Ivashkiv LB. TNF biology, pathogenic mechanisms and emerging therapeutic strategies. *Nat Rev Rheumatol* 2016;12:49-62.
17. Ben-Horin S, Chowers Y. Tailoring anti-TNF therapy in IBD: drug levels and disease activity. *Nat Rev Gastroenterol Hepatol* 2014;11:243-255.
18. Zeissig S, Rosati E, Dowds CM, et al. Vedolizumab is associated with changes in innate rather than adaptive immunity in patients with inflammatory bowel disease. *Gut* 2018.

19. Vétizou M, Pitt JM, Daillère R, et al. Anticancer immunotherapy by CTLA-4 blockade relies on the gut microbiota. *Science* 2015;350:1079-1084.
20. Daillère R, Vétizou M, Waldschmitt N, et al. *Enterococcus hirae* and *Barnesiella intestinihominis* Facilitate Cyclophosphamide-Induced Therapeutic Immunomodulatory Effects. *Immunity* 2016;45:931-943.
21. Walmsley RS, Ayres RCS, Pounder RE, et al. A simple clinical colitis activity index. *Gut* 1998;43:29-32.
22. Yue JC, Clayton MK. A Similarity Measure Based on Species Proportions. *Communications in Statistics - Theory and Methods* 2005;34:2123-2131.
23. Schloss PD, Westcott SL, Ryabin T, et al. Introducing mothur: Open-Source, Platform-Independent, Community-Supported Software for Describing and Comparing Microbial Communities. *Applied and Environmental Microbiology* 2009;75:7537-7541.
24. Dufrene ML, P. Species assemblages and indicators species: the need for a flexible assymetrical approach. *Ecological Monographs* 1997;67:345-66.
25. Magnusdottir S, Heinken A, Kutt L, et al. Generation of genome-scale metabolic reconstructions for 773 members of the human gut microbiota. *Nat Biotech* 2017;35:81-89.
26. Turnbaugh PJ, Hamady M, Yatsunencko T, et al. A core gut microbiome in obese and lean twins. *Nature* 2008;457:480.
27. Rohr RP, Saavedra S, Bascompte J. On the structural stability of mutualistic systems. *Science* 2014;345.
28. Mougi A, Kondoh M. Diversity of Interaction Types and Ecological Community Stability. *Science* 2012;337:349-351.
29. Brandstetter BR, Korfmann A, Kroke A, et al. Dietary Habits in the German EPIC Cohorts: Food Group Intake Estimated with the Food Frequency Questionnaire. *Annals of Nutrition and Metabolism* 1999;43:246-257.
30. Vaahtovuori J, Munukka E, Korkeamäki M, et al. Fecal Microbiota in Early Rheumatoid Arthritis. *The Journal of Rheumatology* 2008;35:1500.
31. Zhang X, Zhang D, Jia H, et al. The oral and gut microbiomes are perturbed in rheumatoid arthritis and partly normalized after treatment. *Nat Med* 2015;21:895-905.
32. Magnusson MK, Strid H, Sapnara M, et al. Anti-TNF Therapy Response in Patients with Ulcerative Colitis Is Associated with Colonic Antimicrobial Peptide Expression and Microbiota Composition. *Journal of Crohn's and Colitis* 2016.
33. Flint HJ, Duncan SH, Scott KP, et al. Links between diet, gut microbiota composition and gut metabolism. *Proceedings of the Nutrition Society* 2015;74:13-22.
34. Louis P, Hold GL, Flint HJ. The gut microbiota, bacterial metabolites and colorectal cancer. *Nat Rev Micro* 2014;12:661-672.
35. Flint HJ, Duncan SH, Scott KP, et al. Interactions and competition within the microbial community of the human colon: links between diet and health. *Environmental Microbiology* 2007;9:1101-1111.
36. Zelezniak A, Andrejev S, Ponomarova O, et al. Metabolic dependencies drive species co-occurrence in diverse microbial communities. *Proceedings of the National Academy of Sciences* 2015;112:6449-6454.
37. Yilmaz B, Juillerat P, Øyås O, et al. Microbial network disturbances in relapsing refractory Crohn's disease. *Nature Medicine* 2019;25:323-336.

38. Hyams JS, Davis Thomas S, Gotman N, et al. Clinical and biological predictors of response to standardised paediatric colitis therapy (PROTECT): a multicentre inception cohort study. *The Lancet* 2019;393:1708-1720.
39. Bauer E, Thiele I. From metagenomic data to personalized in silico microbiotas: predicting dietary supplements for Crohn's disease. *npj Systems Biology and Applications* 2018;4:27.
40. Graspentner S, Waschina S, Künzel S, et al. Gut Dysbiosis With Bacilli Dominance and Accumulation of Fermentation Products Precedes Late-onset Sepsis in Preterm Infants. *Clinical Infectious Diseases* 2018:ciy882-ciy882.
41. Zeissig S, Rosati E, Dowds CM, et al. Vedolizumab is associated with changes in innate rather than adaptive immunity in patients with inflammatory bowel disease. *Gut* 2019;68:25.
42. Häslér R, Sheibani-Tezerji R, Sinha A, et al. Uncoupling of mucosal gene regulation, mRNA splicing and adherent microbiota signatures in inflammatory bowel disease. *Gut* 2016.

Figure Legends

Figure 1: α - and β -diversity of intestinal microbial communities in inflammatory bowel disease (IBD), rheumatic diseases (RD) and healthy control subjects (HC). α -diversity indices as estimated by observed number of phylotypes (A), estimated richness (B), NP Shannon index of diversity (C) and phylodiversity (D). Principal coordinate plots based on Jaccard (E) and Bray-Curtis (F) distances. Significance of differences in α -diversity indices were determined by the Mann Whitney U test. Significance of differences in β -diversity was assessed by PERMANOVA statistics. Bonferroni corrected p values: Bray Curtis: (HC-IBD, $p = 0.0003$; HC-rheumatic diseases, $p = 0.0003$; IBD-rheumatic diseases, $p = 0.0366$); Jaccard (HC-IBD, $p = 0.0003$; HC-rheumatic diseases, $p = 0.0003$; IBD-rheumatic diseases, $p = 0.237$).

Figure 2: Anti TNF therapeutic intervention restores α -diversity in IBD, but not in rheumatic diseases

Observed number of phylotypes (A and E), estimated species richness (B and F), NP Shannon diversity (C and G) and phylodiversity (D and H) indices were assessed in fecal samples collected from patients with IBD or rheumatic diseases (RD) at baseline and after initiation of anti-TNF interventions (W, week). Healthy control subjects (HC) served as benchmark for normal microbial diversities. Remitters are shown as open circles, whereas non-remitters are shown as filled circles. Significance of observed differences were determined by Wilcoxon matched-pairs signed rank test (pairwise comparison: before and after the beginning of therapeutic interventions) or Mann Whitney U test (healthy control subjects compared to patients).

Figure 3: Anti-TNF intervention partly restores phylotype alterations in IBD.

(A) Loss (down) or gain (up) of indicator species status was determined in relation to healthy control group microbiota. Relative abundance signal values were transformed into Z-scores for visualization. Each column represents an individual patient whereas each row represents the relative abundance of labelled indicator species. (B) Representative indicator phylotypes that were significantly decreased at week 0 compared to healthy controls and increased in abundance after anti-TNF therapeutic intervention to become comparable to healthy control subject status (median = green dashed line) at week 30. p-values indicate the statistical significance at week 0 between IBD and healthy control patients.

Figure 4: Bacterial metabolic interactions are disrupted in IBD and rheumatic diseases, and metabolic interchange is especially reduced in patients not remitting in response to anti-TNF intervention.

(A) Fraction of antagonistic (+/-), competitive (-/-) and mutualistic (+/+) interactions among bacterial community members for each disease group (IBD or rheumatic diseases) and therapy duration (week 0, 2, 6, or 30). Dashed lines indicate the median value for samples from healthy subjects and the gray area the interquartile range (IQR). (B) Predicted total intercellular metabolite fluxes (i.e. interchange/cross-feeding) of all metabolites relative to healthy controls. The dashed line (=1) indicate the median value and the gray area the IQR for samples from healthy subjects. Bar heights denote the median interchange estimates for the respective disease group (pre-treatment vs. post-treatment), depending on the patients' therapy response status (Remission vs. No Remission). Error bars span the IQR. Asterisks indicate significantly different

levels for the respective disease group and time compared to healthy controls (two-sided Mann-Whitney U test, $p < 0.05$).

Figure 5: *In silico*-predicted ecological interaction types and total metabolite interchange levels in patients with IBD before and during anti-TNF intervention.

Fraction of antagonistic (+/-), competitive (-/-) and mutualistic (+/+) interactions among bacterial community members. Dashed lines indicate the median value for samples from healthy subjects and the gray area the interquartile range (IQR). (B) Predicted total intercellular metabolite fluxes (i.e. interchange/cross-feeding) of all metabolites relative to the interchange levels in healthy controls. The dashed line (=1) indicates the median value and the gray area the IQR for samples from healthy subjects. Bar heights denote the median of predicted interchange estimates for the respective disease group and the patients' remission status. Error bars span the IQR. Asterisks indicate significantly different levels for the respective disease group and time compared to healthy controls (two-sided Mann-Whitney U test, $p < 0.05$).

Figure 6: Disruption of specific metabolite exchange interactions between bacteria is more pronounced in non-remitter patients with IBD than in remitter patients already prior to anti-TNF therapy.

The Venn diagrams show metabolites whose exchanges between bacterial community members are, compared to healthy controls, significantly reduced in patients with IBD who go into remission and/or do not achieve remission in the course of the treatment (left: before treatment; right: after treatment. False discovery rate-corrected two-sided Mann-Whitney U test, $p < 0.05$).

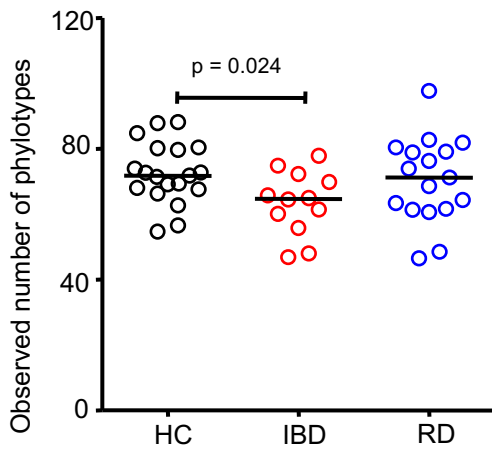
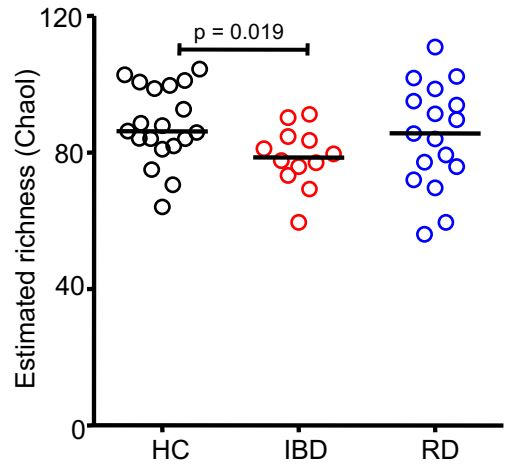
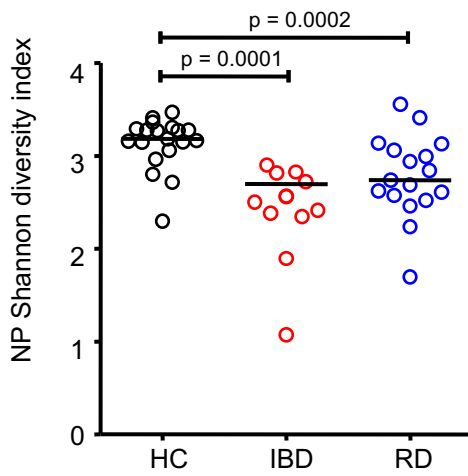
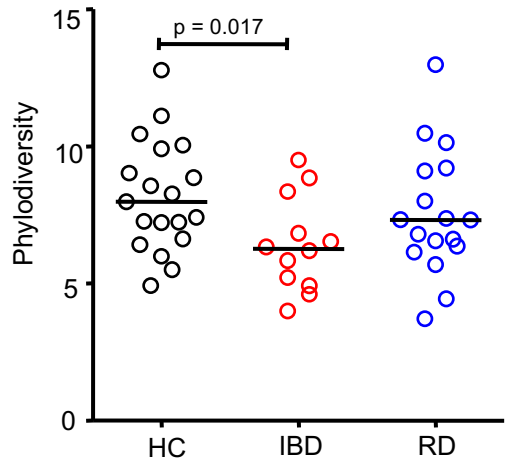
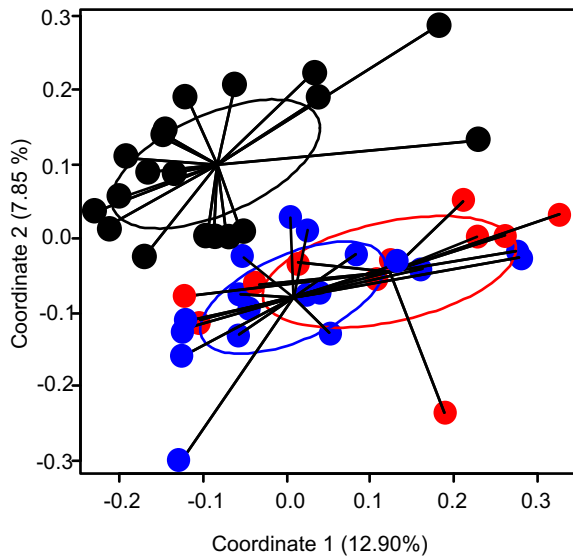
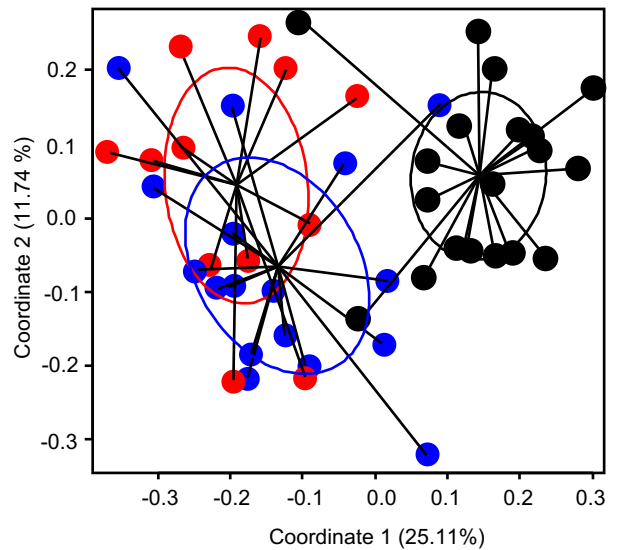
All anti-TNF-treated patients with IBD from cohort #1 and #2 were combined for this analysis to improve statistical power.

Figure 7: Stool metabolome analysis identifies indicator metabolites of therapy response in patients with IBD

Orthogonal partial least squares discriminant analysis (OPLS-DA) scores plot derived from (+)- (A) and (-)-HILIC-LC-MS/MS (B) analysis of longitudinal stool samples of 9 patients with IBD, who underwent anti-TNF therapy. Samples were collected before therapy and at 14 weeks. Baseline, non-remission and remission samples are coloured in gray and red respectively. OPLS-loading plot illustrates clusters, which are responsible for the separation of the three groups. (C) Clusters are coloured according to the importance for the three classes (red (high) to gray (low)). Metabolites identified by authentic chemical standards are labelled. (D–F) Creatinine, butyric acid and the metabolite Cluster_1061 were found to be significantly altered between the groups. #: increased at baseline compared to the non-remission group; *: increased in the remission group compared to baseline; +: increased in the nonremission group compared to remission group; significance was calculated with Mann-Whitney rank sum test (p-value<0.05).

ACKNOWLEDGEMENTS

The authors thank all the participating patients for supporting this study by donating biomaterial. The expert technical assistance by Karina Greve and Dorina Oelsner as well as the scientific support by Markus Schilhabel and Sören Franzenburg are gratefully acknowledged. We thank Ines Thiele, Eugen Bauer and Almut Heinken for valuable discussions concerning constraint-based modeling of microbial communities.

A**B****C****D****E****F**

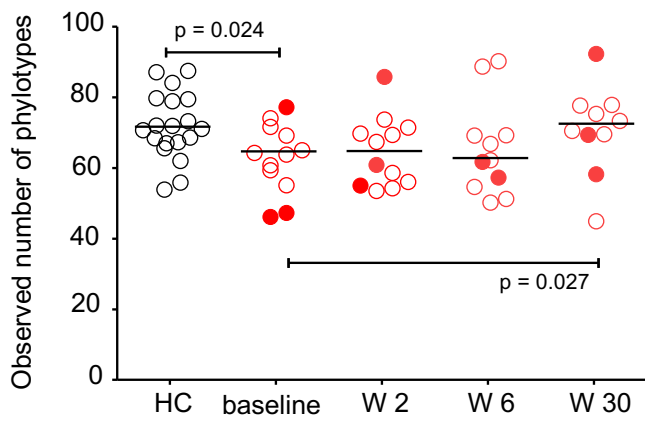
● Healthy controls

● Inflammatory bowel disease

● Rheumatic disease

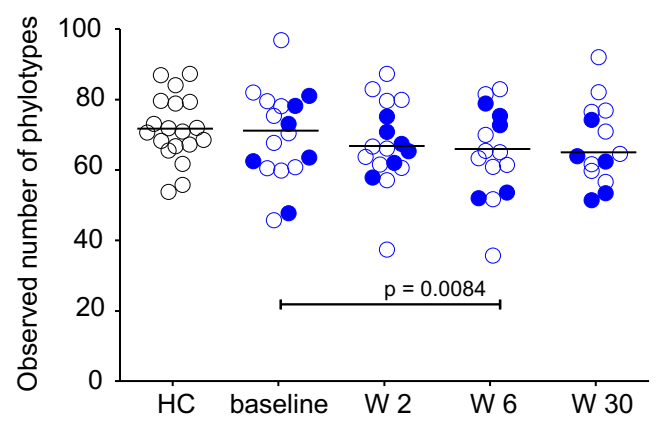
○ healthy controls
 ○ remitting IBD
 ● non-remitting IBD

A

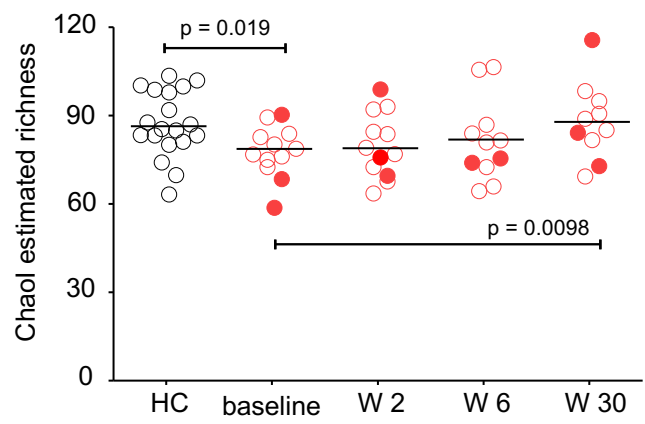


○ healthy controls
 ○ remitting RD
 ● non-remitting RD

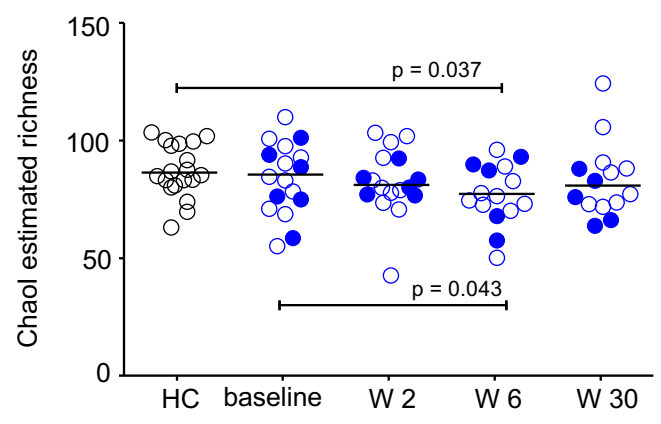
E



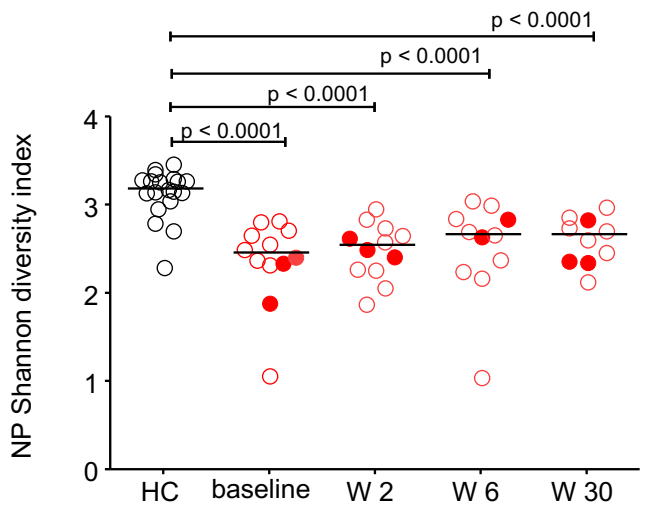
B



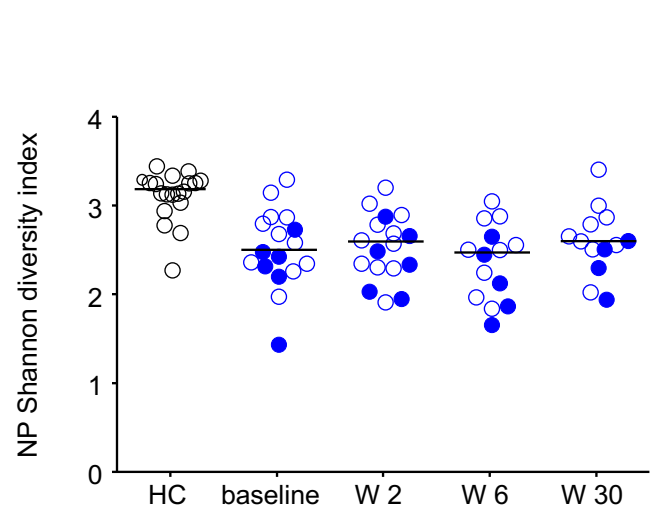
F



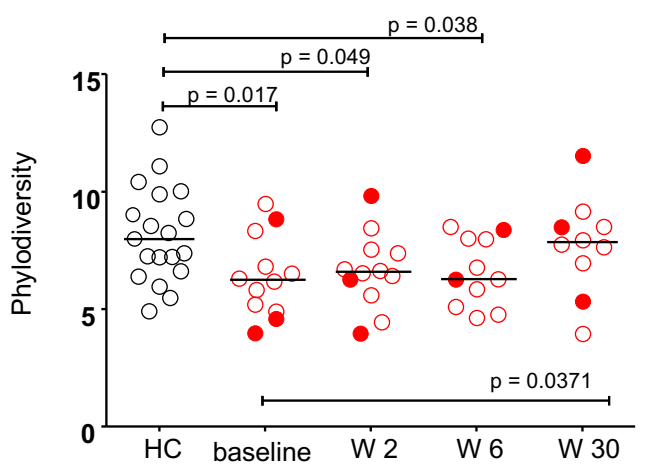
C



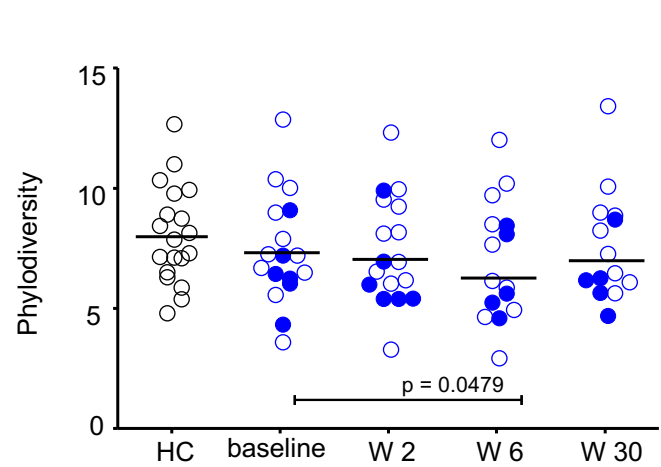
G

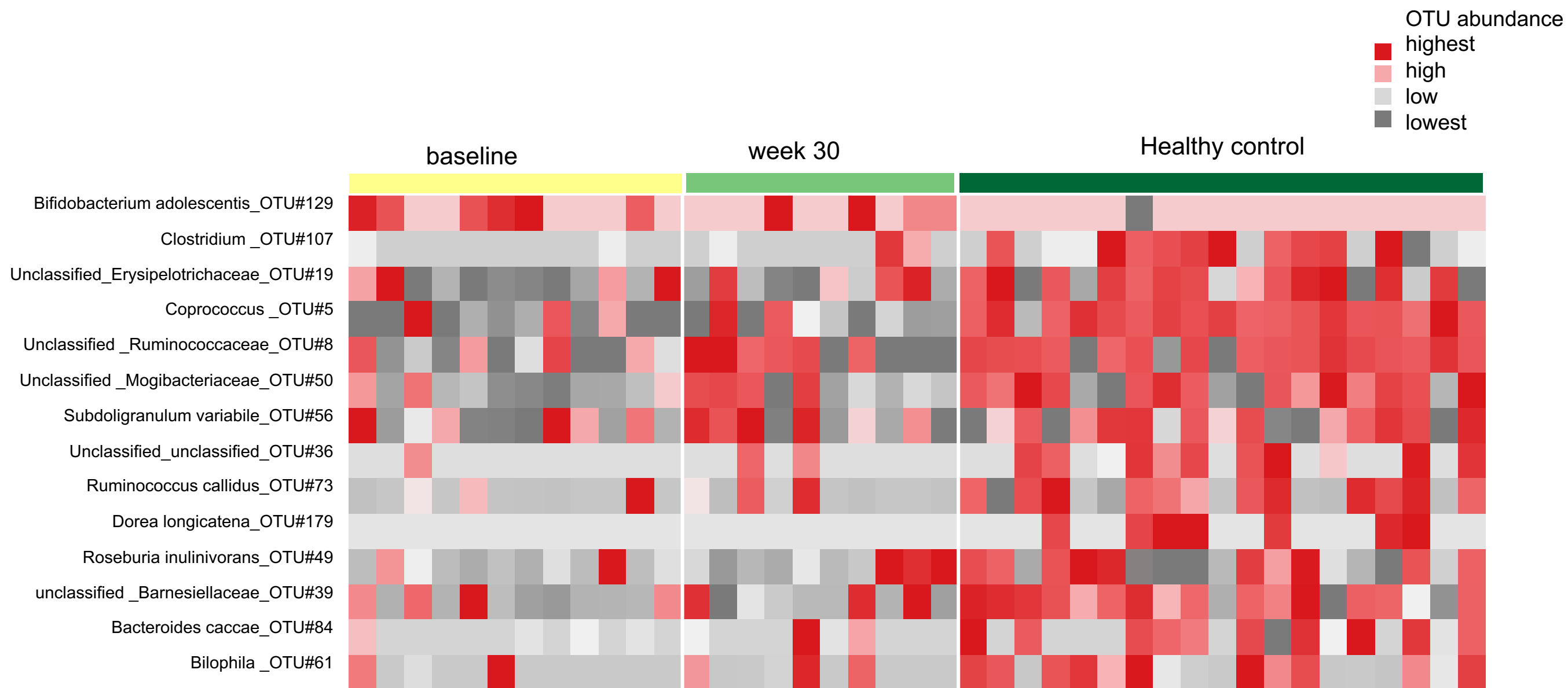
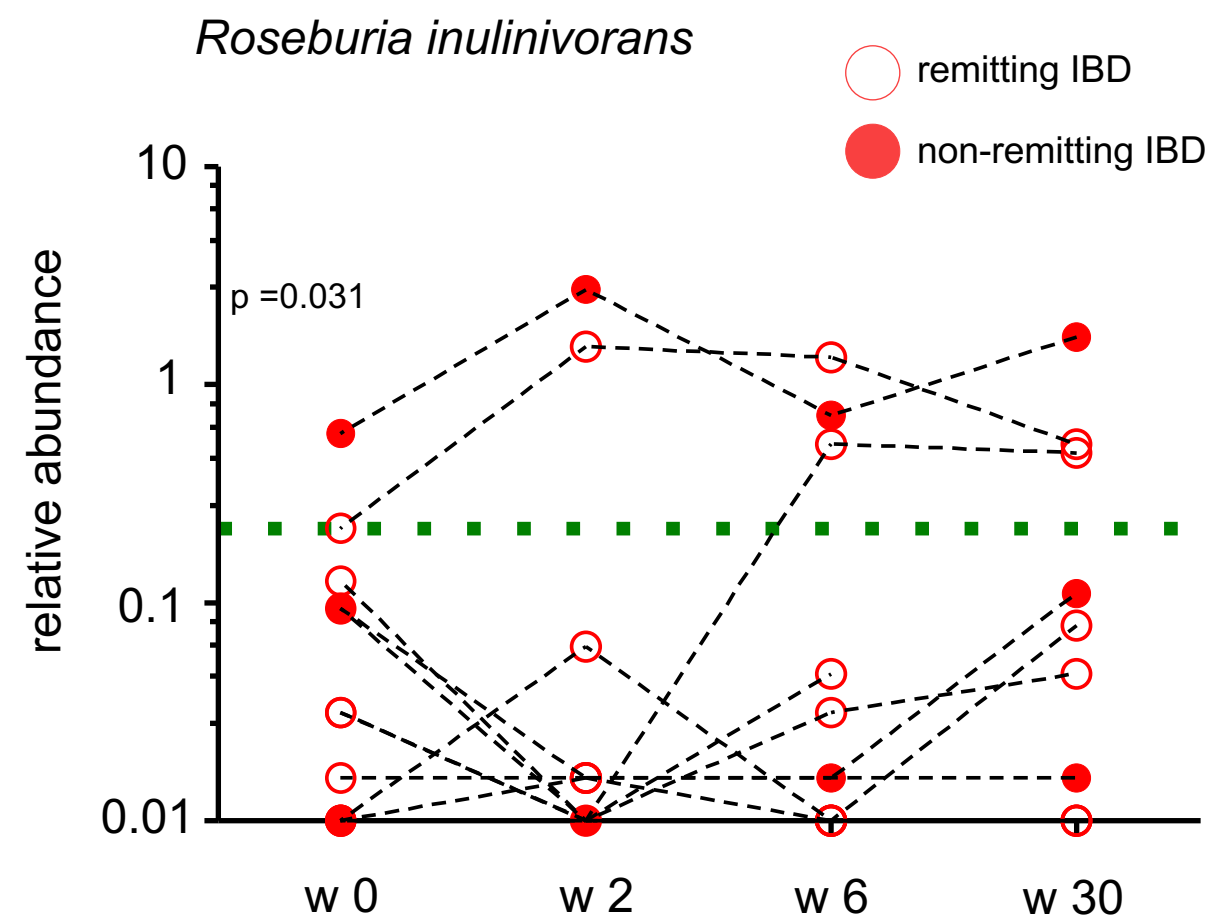
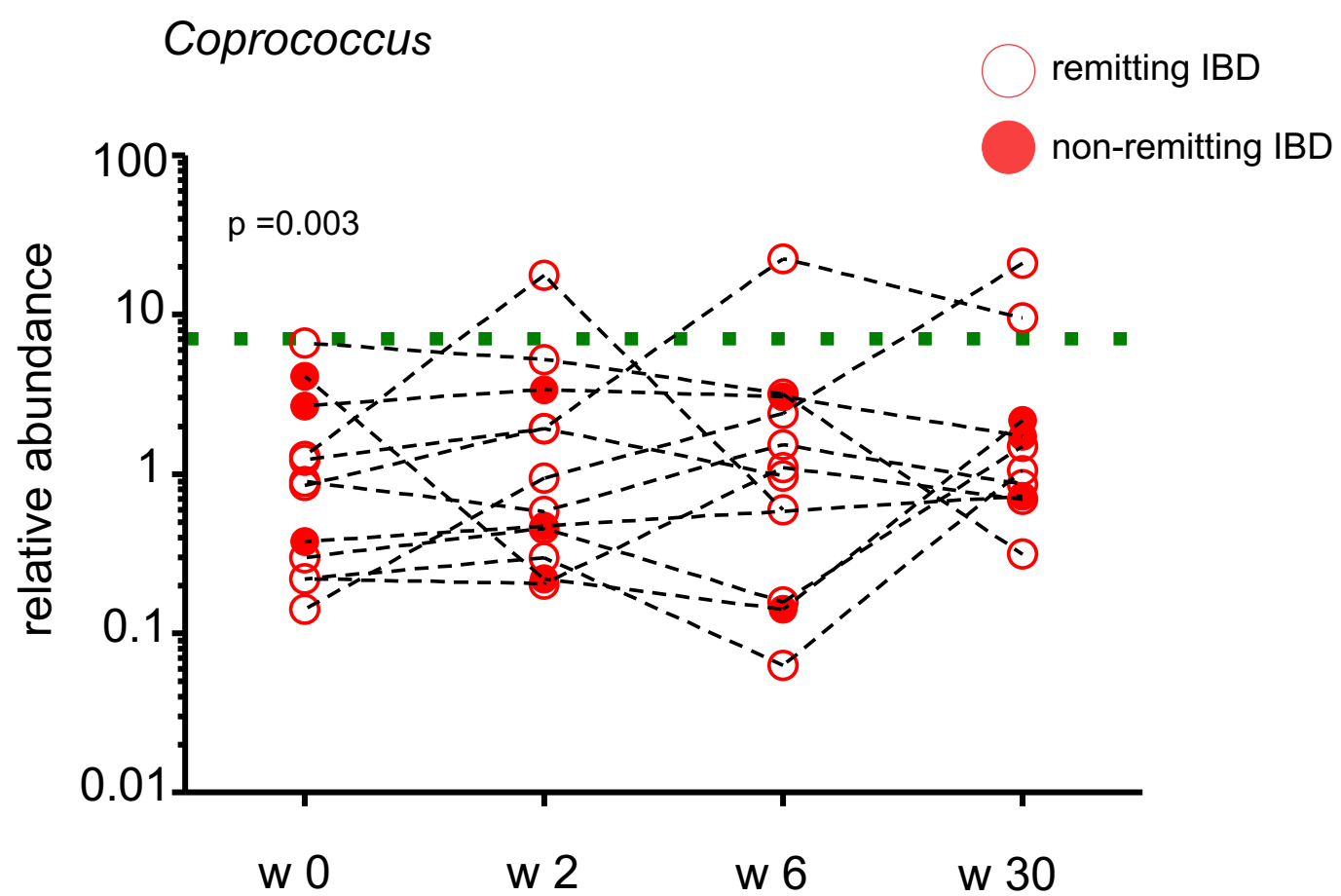


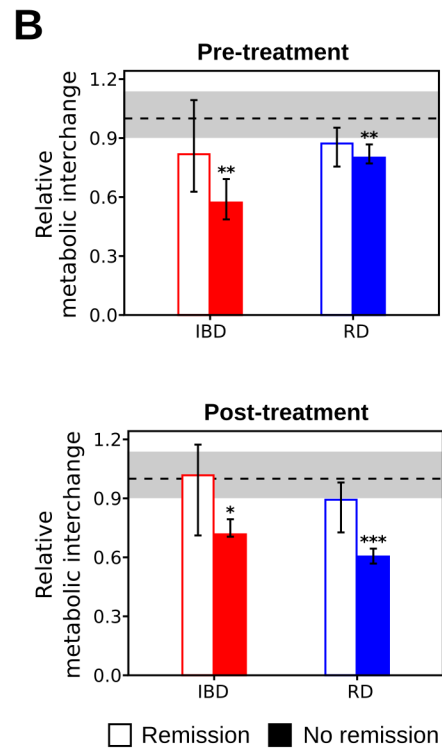
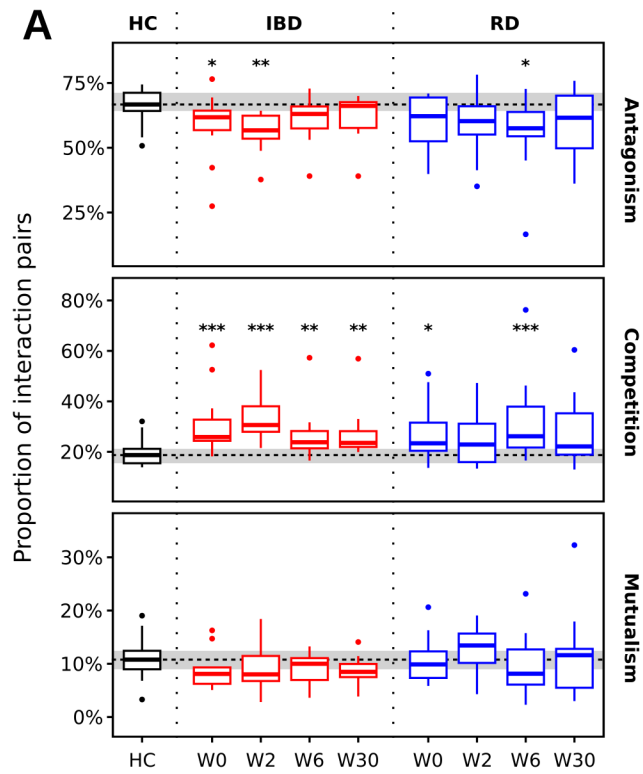
D

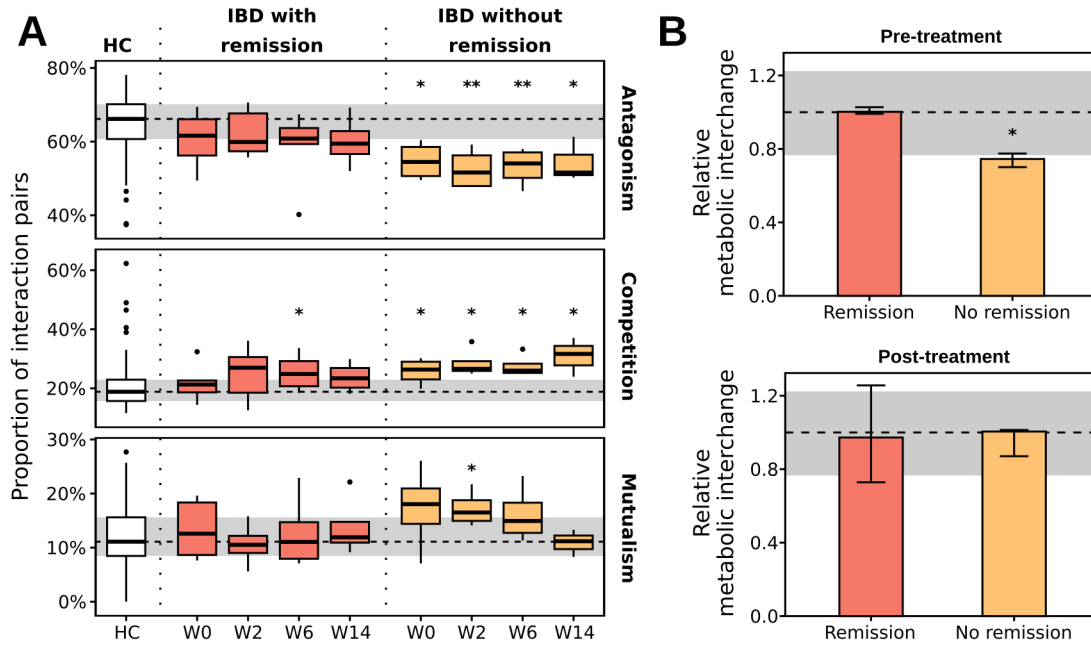


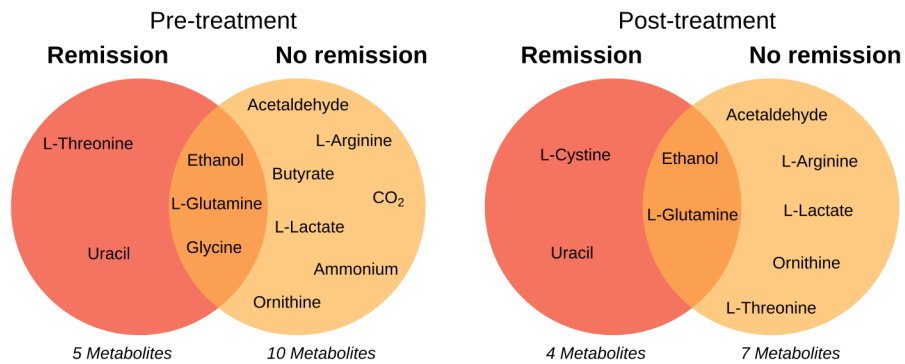
H



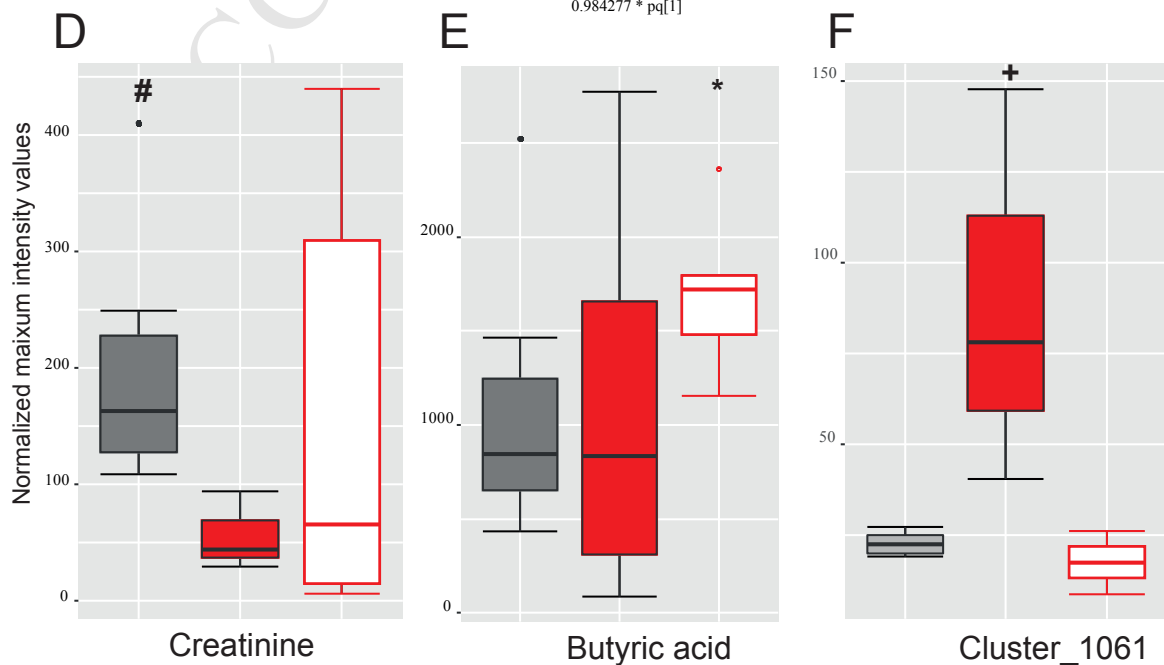
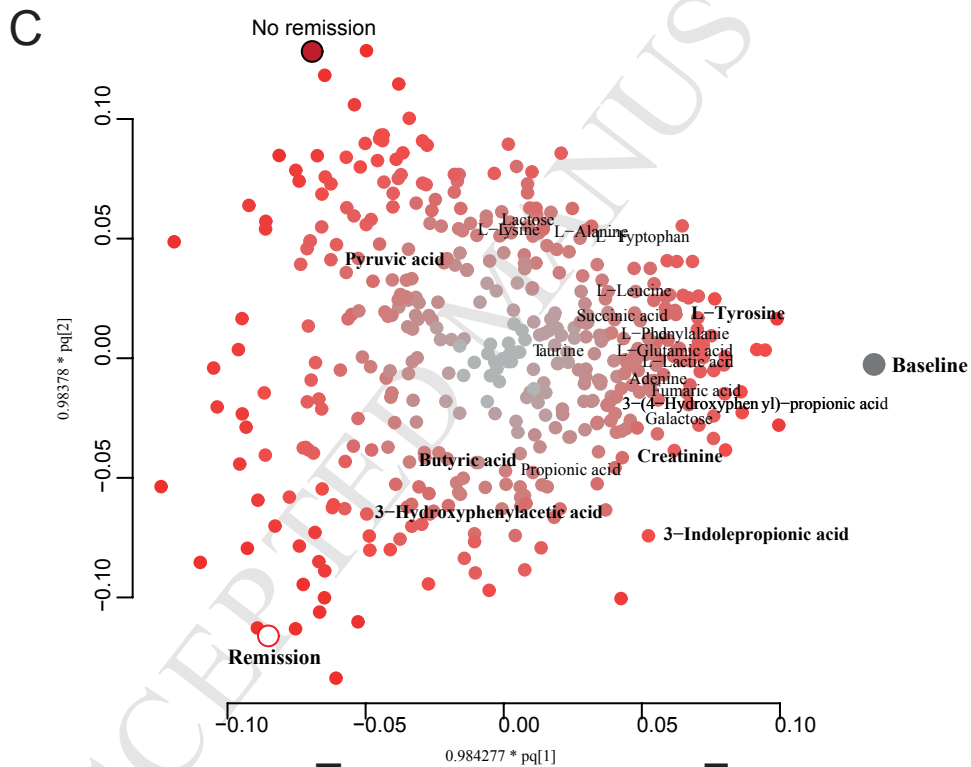
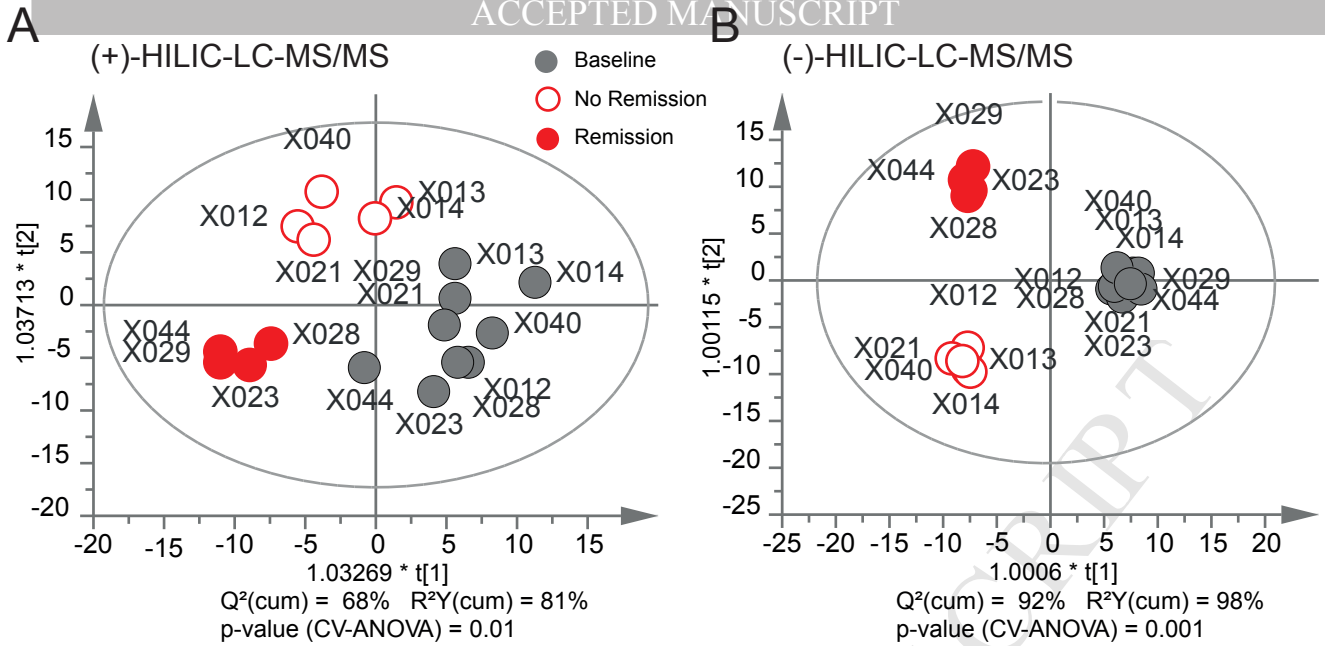
A**B**







ACCEPTED MANUSCRIPT



What you need to know

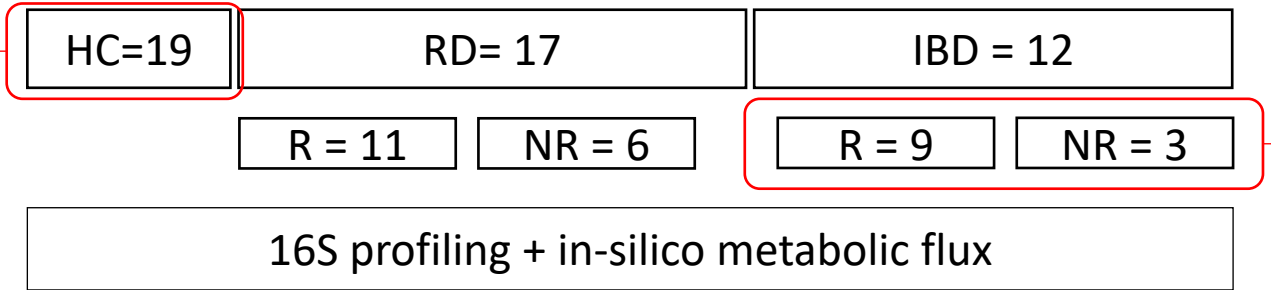
Background: We investigated the effects of treatment with tumor necrosis factor antagonists (anti-TNF) on gut microbe community structure and function in patients with inflammatory bowel diseases (IBD). We analyzed patterns of metabolites in fecal samples before and after anti-TNF therapy.

Findings: Anti-TNF therapy shifted the diversity of fecal microbiota in patients with IBD toward that of healthy individuals. Levels of butyrate and substrates involved in butyrate synthesis were significantly associated with clinical remission following anti-TNF therapy.

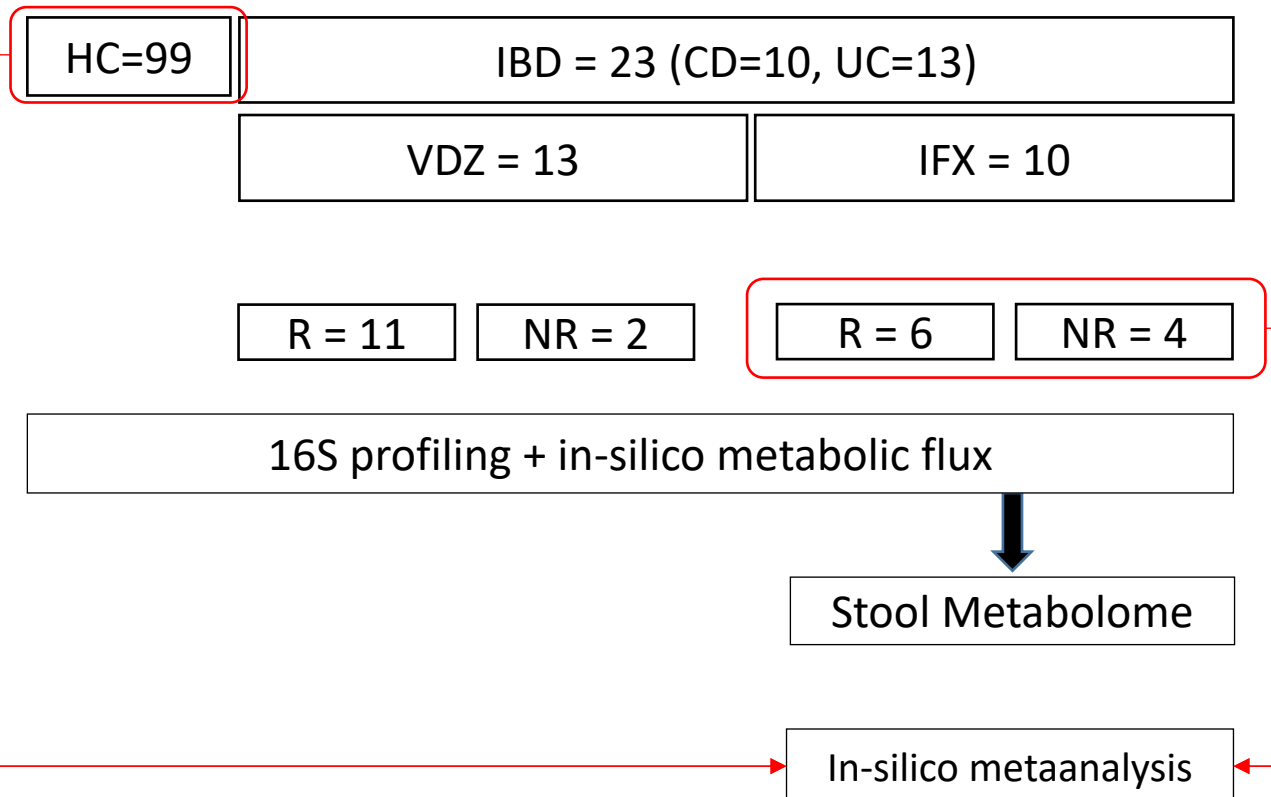
Impact: In silico modelling of metabolic profiles of fecal samples might be used to identify patients with IBD likely to achieve remission following anti-TNF therapy. These analyses might also provide information about the pathogenesis of IBD.

Lay Summary: In patients with inflammatory bowel diseases, treatment with drugs such as tumor necrosis factor antagonists alters the collection of gut microbes to more closely resemble that of healthy persons. We identified molecules produced by these microbes that are associated with response to therapy. This finding might be used to improve IBD treatment.

Cohort #1

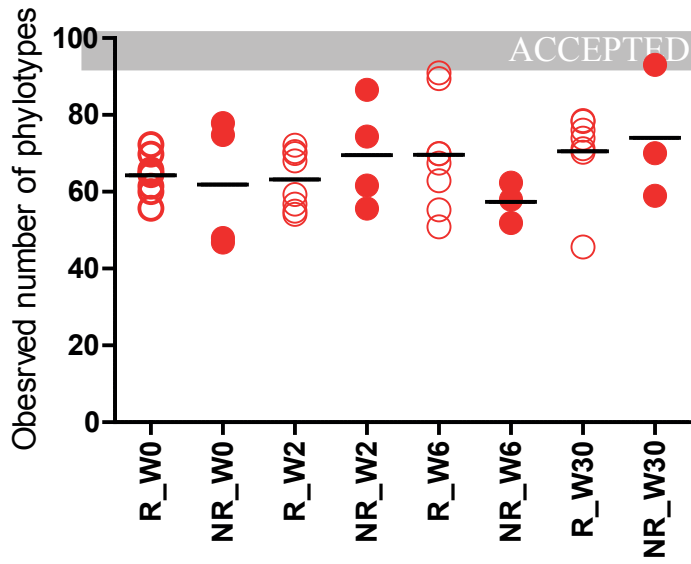


Cohort #2

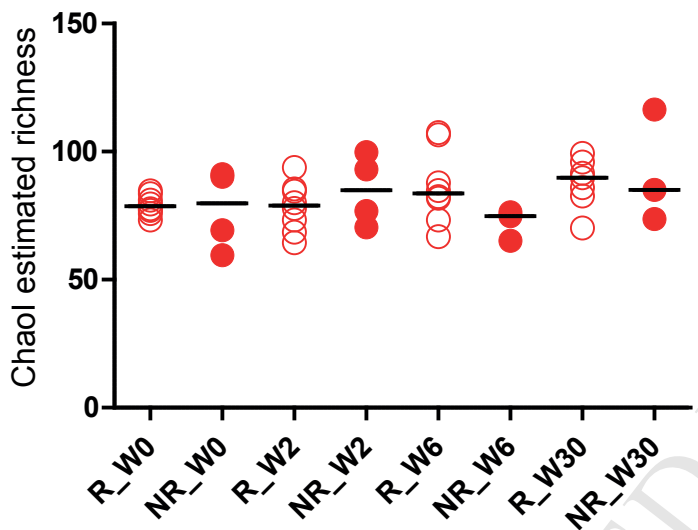


IBD

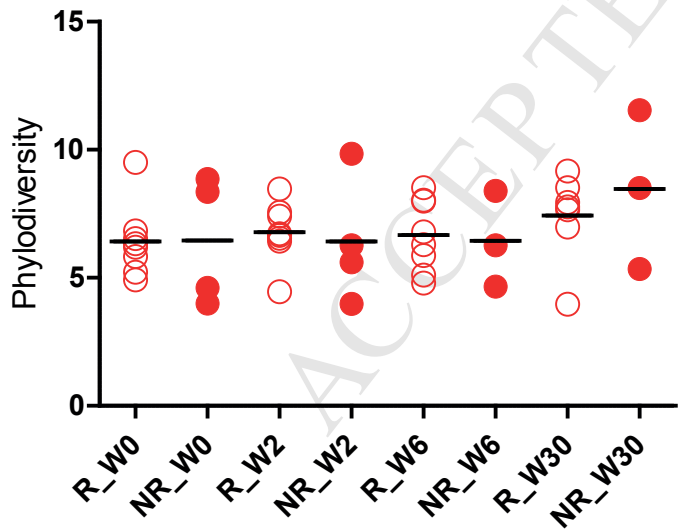
A



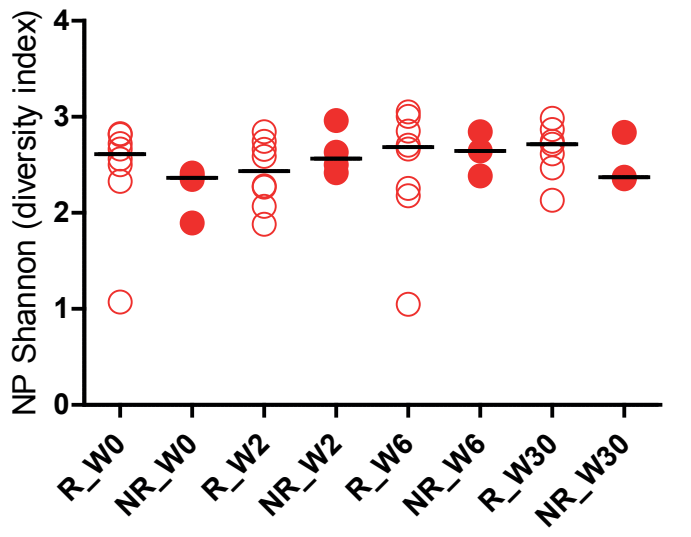
C



E

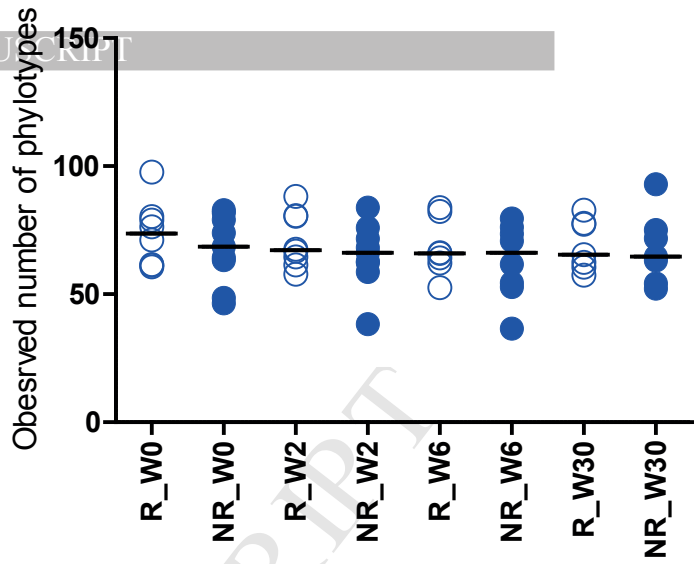


G

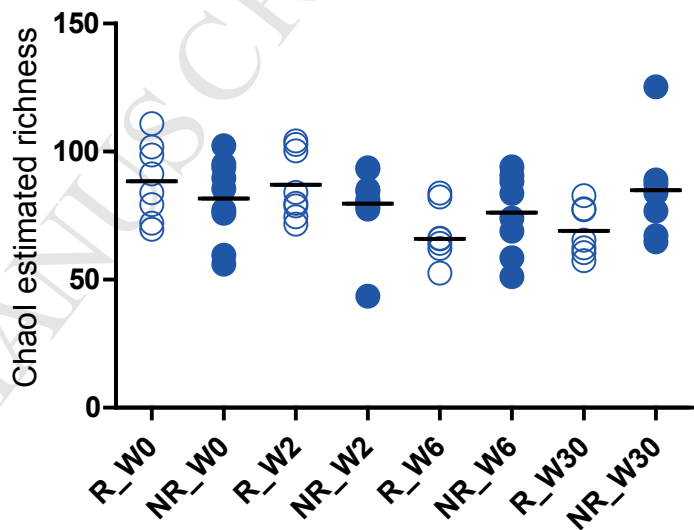


RD

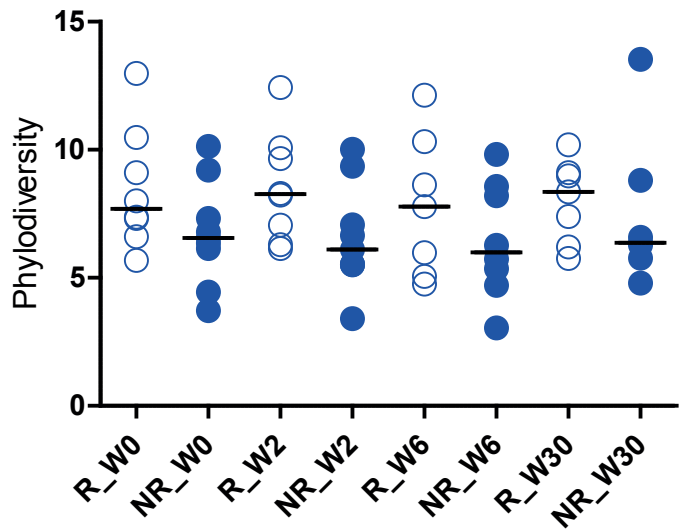
B



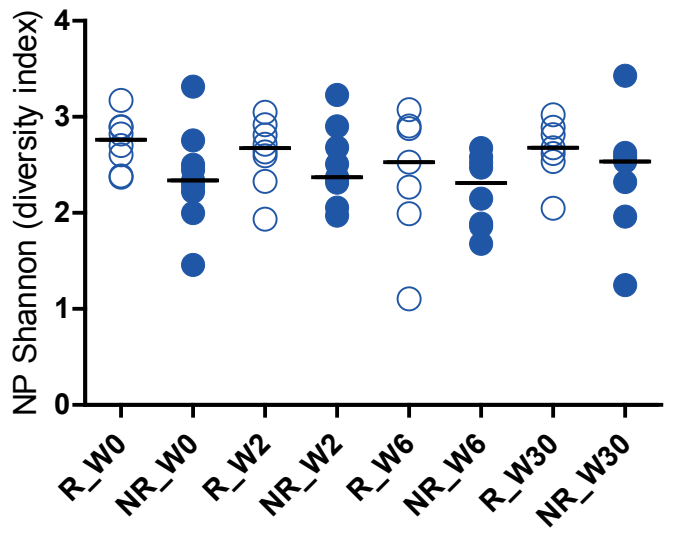
D

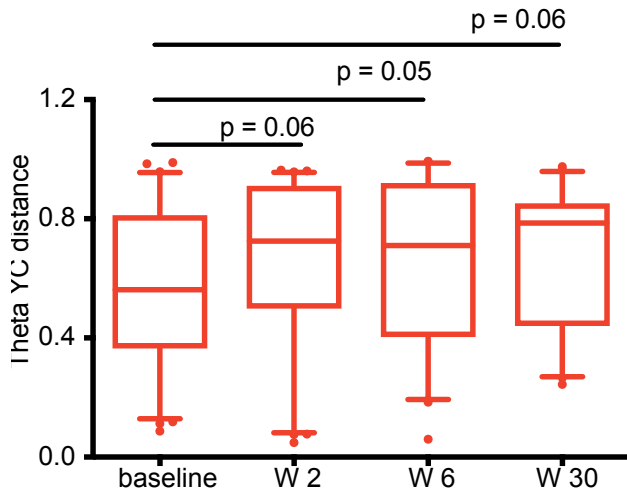
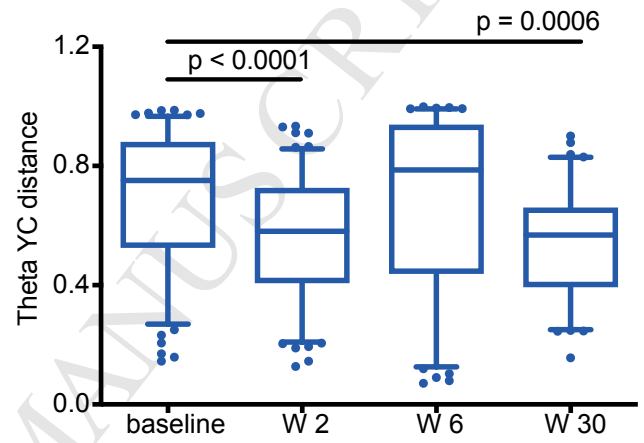
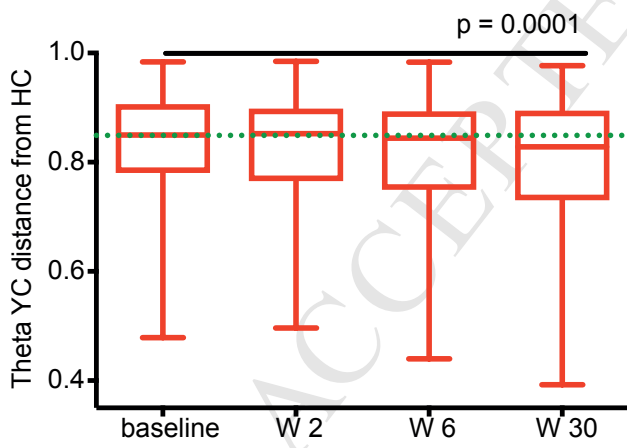
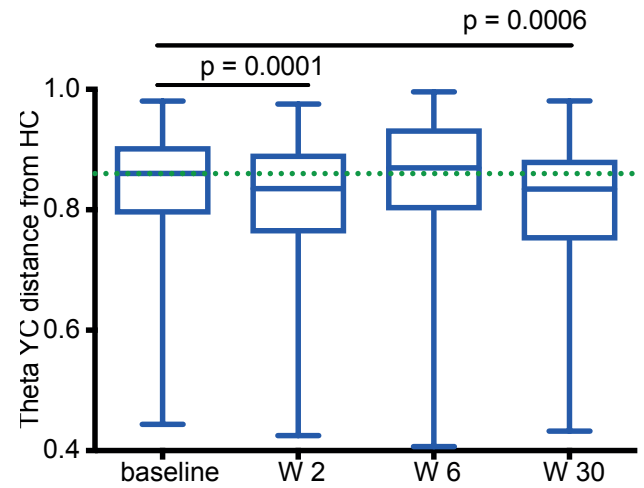


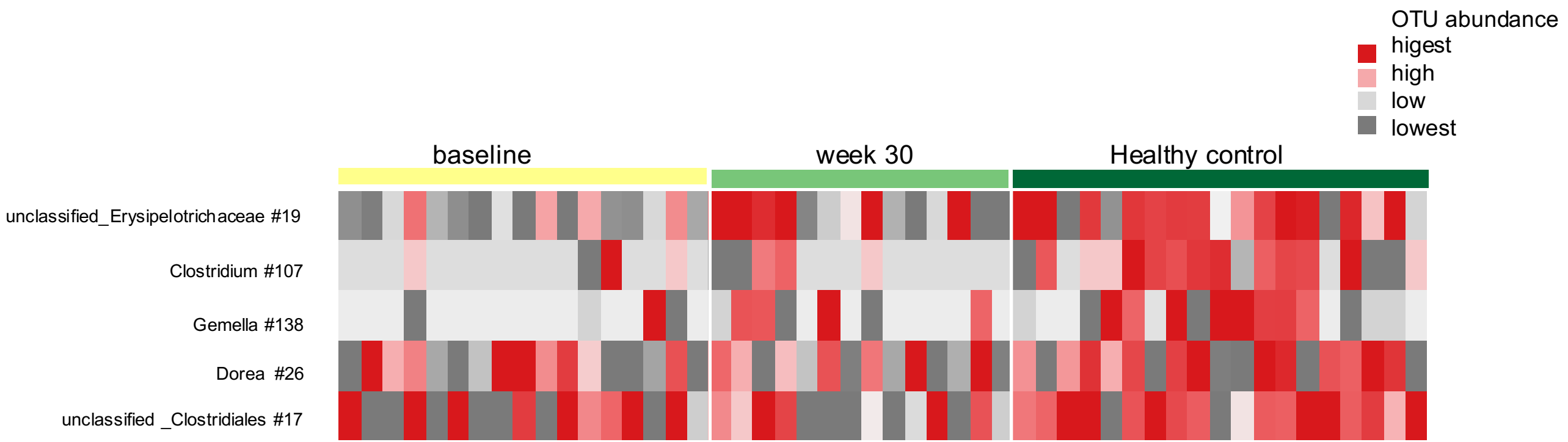
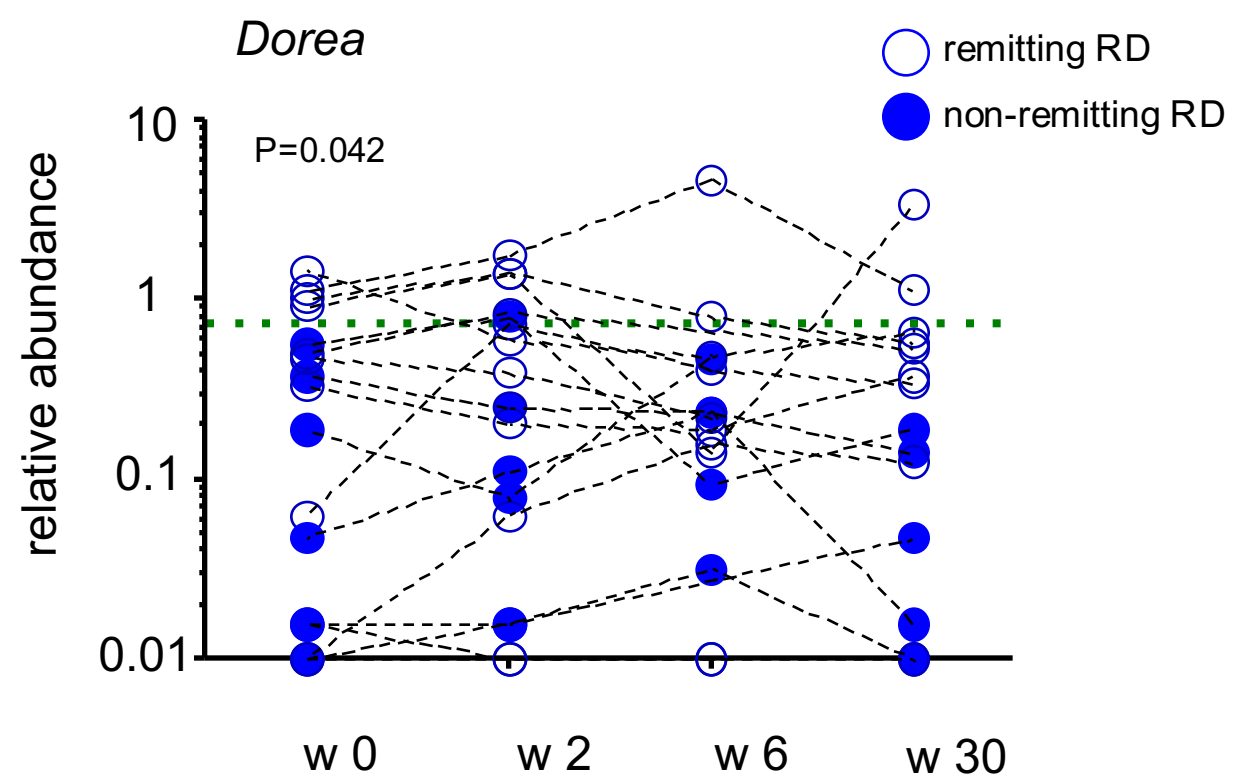
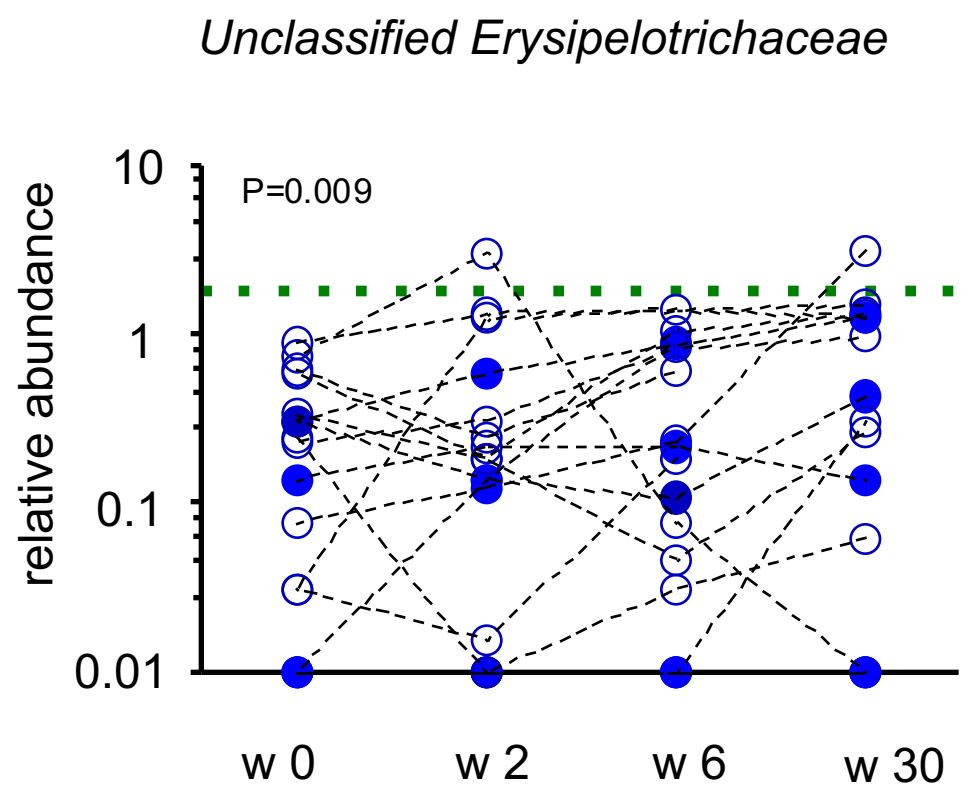
F

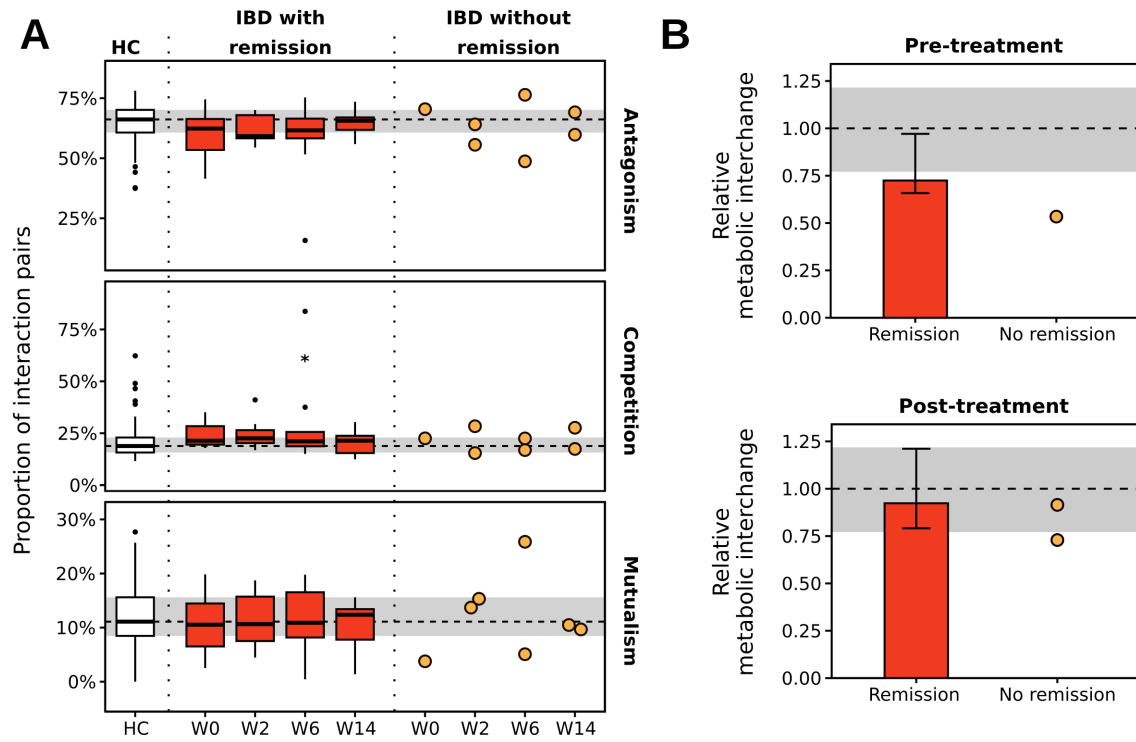


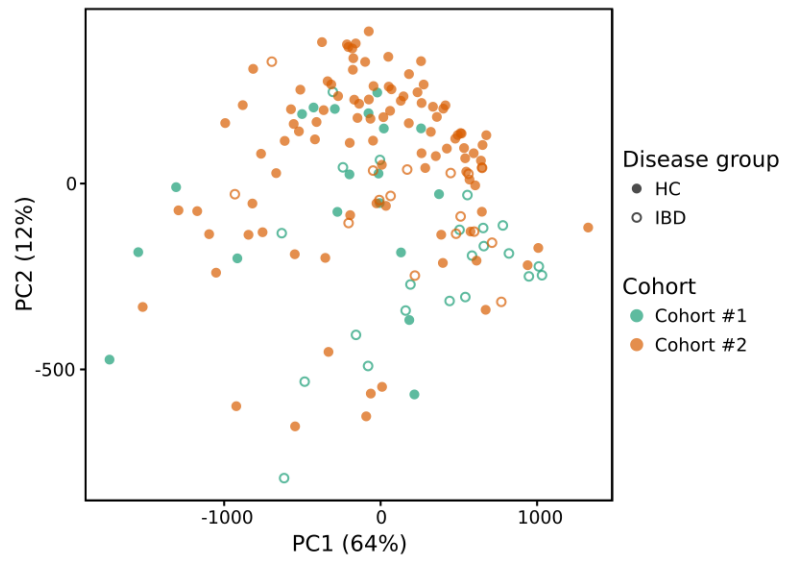
H



A**B****C****D**

A**B**





ACCEPTED MANUSCRIPT

Aden K. , Rehman A. , Waschina S. et. al.: Gut microbial metabolic functions are associated with Anti-TNF efficacy in IBD patients

Supporting Document

Supplementary Figures**Figure S1: Schematic overview of included cohort and analysis workflow**

For hypothesis generation cohort #1 (MAUT) was included in 16s profiling + in-silico metabolic flux analysis. Key findings were validated in cohort #2 (EMED). For in-silico metaanalysis (Figure 6) HC (in total n=118) and IBD patients (in total n=35) were pooled from cohort #1 and #2.

Figure S2: Alpha diversity in IBD and RD patients according to responder status.

As a measure of change in alpha diversity, observed number of phylotypes (A and B), estimated species richness (C and D), phylo-diversity (E and F) and NP Shannon diversity (G and H) were assessed in faecal samples collected from IBD and RD subjects at baseline and after initiation of anti TNF α interventions. Responders are shown as open circles, whereas non-responders are shown as filled circles.

Figure S3: Anti TNF α therapeutic intervention induces expansion of beta-diversity in IBD but not in RD

Yue and Clayton dissimilarity (beta diversity) within IBD (A) and RD (B) groups before and after anti TNF α interventions. Interindividual distances before therapy initiation were used as baseline point to compare interindividual distances at week 2, week 6 and week 30 after **anti TNF α** intervention. p values were determined by Wilcoxon matched-pairs signed rank test and represent Yue and Clayton dissimilarity between healthy control and IBD patients (C), healthy control and RD (D). Interindividual distances were compared to healthy control at baseline and after therapy initiation at week 2, week 6 and week 30. Significance of changes were ascertained by Mann Whitney test

Figure S4: Indicator phylotypes before and after anti TNF α therapeutic intervention in RD patients.

(A) Loss (down) or gain (up) of indicator species status was determined in relation to healthy control group microbiota. Relative abundance signal values were transformed in to Z-score for visualization. Each column represents individual patients whereas each row represents the relative abundance of labelled indicator species. (B) Representative indicator phylotypes, that were significantly decreased at week 0 compared to healthy control and increased in abundance after anti TNF α therapeutic intervention to become comparable to healthy control subject status at week 30. P-values indicate the statistical significance at week 0 between RD and HC patients.

Figure S5: Linear regression analysis of gut metabolic interchange with disease activity parameters at baseline.

Linear regression of relative metabolic interchange with Disease activity score (HBI/Mayo), Leukocytes count, C-reactive protein and pathology index. Note, that none of the listed parameters shows a significant relationship with the degree of relative metabolic interchange in baseline microbial samples.

Figure S6: In silico-predicted ecological interaction types and total metabolite interchange levels in IBD patients upon ant- $\alpha 4\beta 7$ integrin intervention.

Fraction of antagonistic (+/-), competitive (-/-), and mutualistic (+/+) interactions among bacterial community members. The dashed line indicates the median value for samples from healthy subjects and the gray area the interquartile range (IQR). (B) The predicted total intercellular metabolite fluxes (i.e. interchange/cross-feeding) of all metabolites relative to the interchange levels in healthy controls. The dashed line (=1) indicates the median value and the gray area the IQR for samples from healthy

subjects. Bar heights denote the median of predicted interchange estimates for the respective disease group and the patients' remission status. Error bars span the IQR.

Figure S7: Principle component analysis on predicted metabolite exchange rates.

Samples from healthy controls and IBD patients (pre-treatment only) and from both cohorts (MAUT and EMED) were combined for this analysis. The analysis included the in silico-predicted cross-feeding rates of 374 different metabolites. Shown are only the first two principle component axes, which cover 78% of the observed variability in the data.

Supplementary Tables

Table S1: Patient characteristics of cohort #1

Table S2: Response status in IBD and RD patients from cohort #1

Table S3: Remission status in IBD patients from cohort #2

Table S4: Distribution of bacterial phylotypes in fecal samples obtained from healthy subjects and IBD and RD subjects in cohort #1.

See online version for download

Table S5: Indicator value and p values of phylotypes altered positively or negatively after 30 weeks of anti-TNF α therapeutic intervention in IBD in comparison to healthy subjects.

Table S6: Indicator value and p values of phylotypes altered positively or negatively after 30 weeks of anti-TNF α therapeutic intervention in RD in comparison to healthy subjects.

Table S7: Distribution of bacterial phylotypes in fecal samples obtained from healthy subjects and IBD in cohort #2.

See online version for download

Table S8: List of identified metabolites in (+)/(-)-HILIC-LC-MS/MS

See online version for download

Supplemental Materials and Methods

16S rRNA gene sequencing

Aliquot of extracted DNA was used to amplify V4 variable region of 16S rRNA gene. Forward primer (515F) consists of 5' illumina adaptor (AATGATACGGCGACCACCGAGATCTACAC), a primer pad (TATGGTAATT), linker (GT) and 16S rRNA gene specific forward primer (GTGCCAGCMGCCGCGGTAA) and reverse primer (806R) includes reverse complement of 3' Illumina adapter (CAAGCAGAAGACGGCATACGAGAT) barcode (xxxxxxxxxxxx) reverse primer pad (AGTCAGTCAG), reverse primer linker (CC) and reverse primer (GGACTACHVGGGTWTCTAAT). 16S rRNA gene variable region V3 and V4 will be amplified using dual indexed fusion primers¹, in brief primers consist of illumina linker sequence, 12 base barcode sequence and heterogeneity spacer followed by either 16S rRNA gene specific forward (319F: ACTCCTACGGGAGGCAGCAG) or reverse (806R: GGACTACHVGGGTWTCTAAT) primer sequences. Amplification was performed by Phusion[®] Hot start Flex 2X master Mix (New England Biolab, Germany) in GeneAmp PCR system 9700 (Applied Biosystems, Foster City, California, USA) using following cycling conditions: an initial denaturation of 3 min at 98°C followed by 30 cycles, denaturation at 98°C for 10 seconds, annealing at 55°C for 30 seconds, elongation at 72°C for 30 seconds and a final extension at 72°C for 10 minutes. PCR performance for quality (expected amplicon size) and quantity (band intensity) was assessed by running aliquot of amplified products on agarose gel. Quantitative normalization was performed using SequalPrep kit (Invitrogen) to pool equal amount of amplicons per sample. Sequencing was performed using the Illumina MiSeq platform employing a paired end approach with two times 250 bases, aiming at a 250 base target region. Consequently, this approach ensures the highest contig quality possible.

DNA extraction and 16S rRNA gene sequencing

16S rRNA gene variable region V4 19 (cohort #1) and V3-V420 (cohort #2) based bacterial profiles were generated from IBD and RD patients and control healthy subjects feces. Total genomic DNA was extracted from feces using MoBio Powersoil DNA Isolation kit (Dianova GmbH, Hamburg,

Germany) as per the manufacturer instructions. 16S rRNA gene amplicon libraries were prepared and sequenced as published earlier.

16S rRNA gene sequence analysis

Sequencing reads were primarily processed for quality control using the software mothur package 21. For cohort #1 over 2.2 million high quality reads varying from 6366 to 67699 reads per samples. These sequences were binned into 453 taxonomical phylotypes. For subsequent analysis sequences per sample were rarefied to 6366 to have comparable sequencing depth. This resulted in the rarefication of 388 phylotypes. For cohort #2 over 2.7 million high quality ready varying from 4036 to 43033 reads per samples. These sampels were binned into 441 taxonomical phylotypes. Forward and reverse reads (fastq) were merged to form contigs, and discarded if, were more than 275 bases in length, having any ambiguous base or more than 8 homopolymers. Sequences were aligned against mothur curated silva alignment database and screened to have alignment in amplified specified (V4, V3-V4) regions only. Chimeric sequences were detected by Uchime 22 algorithm and were also removed. In the first step, sequences were classified (threshold 80%) phylogenetically using mothur formatted greengenes (gg_13_8_99) training sets and eliminated if classified as unknown, archaea, eukaryotes, chloroplast or mitochondria. Subsequently, reference-based (green genes) operational taxonomical units (OTUs or phylotypes) picking approach was implemented to cluster sequences with same phylogenetic affiliations in to a phylotype (label=1)²⁻⁵. Alpha diversity indices including observed and estimated number of phylotypes and non-parametric Shannon index were calculated using mothur. For phylogenetic diversity estimation neighbor joining phylogenetic tree was generated by Clearcut command as implemented in mothur. Significance of differences in diversities between healthy, IBD and RD subjects were assessed by Whitney U test, otherwise significance of differences in diversities before and after therapies were assessed by Wilcoxon matched-pairs signed-rank test. Both tests were performed in GraphPad prism 5.0. To identify the specific phylotypes that alters after therapy initiations, we used indicator species analysis²⁴ using 1000 iteration using mothur.

Microbial community modelling

We used a flux balance analysis-based community modelling approach⁶ to assess the functional consequences of shifts in microbial community structure in inflammatory diseases. Flux balance analysis is a methodological framework that tries to infer fluxes within metabolic networks through the utilization of comprehensive reconstructions of an organism's metabolic network and the assumption of evolutionary objectives for inferring fluxes within this network. The underlying metabolic networks used are typically build from the annotated genome of an organism with a downstream manual curation procedure that corrects errors in the model (e.g. based on literature data), removes gaps in metabolic pathways and performs distinct validation steps depending on the amount of experimental data available for a specific organism⁷. Additionally, these networks contain information about the reversibility of the present reactions and information about the specific nutritional environment of an organism that is implemented through constraints on specific metabolite uptake and secretion reactions. Using such networks, flux balance analysis assumes that all (internal) metabolites within a metabolic network are balanced in their production/consumption and that irreversible reactions are only used in the thermodynamically feasible direction. Using this assumption, flux balance analysis determines a flux that maximizes the production of all biomass components from the constrained nutrient supply, which should reflect the evolutionary objective of maximizing growth rate. In the context of microbial community modelling, the metabolic networks of distinct bacterial species are connected to each other through a common compartment that allows for the exchange of metabolites and contains an inflow of metabolites representing the respective growth environment considered (e.g. a specific diet). We here assume that within a community, the objective of optimization is community growth, that is, the maximization of the total amount of bacterial biomass that is being produced⁸.

We used the AGORA (Assembly of Gut Organisms through Reconstruction and Analysis) resource containing genome-scale metabolic models of 773 constituent bacterial species of the human gut microbiota⁸ to predict the ecological relationships between the species that are present in the analysed microbial communities. These models were built in a semi-automated fashion from the annotated genomes of the corresponding species⁸. Furthermore, the models were used to assess the metabolic

activity of communities in the individual samples under defined dietary conditions and oxygen regimes⁸. To simulate the nutritional environment in the human gut, the inflow of metabolites into the models were constrained by assuming a western diet and anaerobic conditions⁸.

Please note that in this study, the bacterial genome-scale metabolic models were used to predict metabolic phenotypes of bacterial populations within the sampled microbiomes. Therefore, predictions should be considered as novel hypothesis on the biochemical physiology of dysbiosis and need to be experimentally scrutinised in future studies.

Prediction of bacterial growth and ecological relationships

In order to determine whether pairs of co-existing species affect each other's metabolism and growth we used Flux Balance Analysis⁹ to predict the organisms' growth rates in isolation (single growth μ_{sg}) and their growth rates in pairs of different species (co-growth μ_{cg}). The underlying rationale is that the growth rate of an organism can be altered through metabolic interactions with neighboring cells. For co-growth simulations, the models were merged in a pairwise manner as previously described^{8,10}. The predicted single growth and co-growth rates were compared to infer the theoretical ecological relationship of each pair of species: The relationship of two bacterial organisms was considered (i) *mutualistic* if each organism could grow faster in co-growth compared to single growth ($\mu_{cg} > \mu_{sg} + \epsilon$), (ii) *competitive* if both organisms grew slower compared to their respective single growth rate ($\mu_{cg} < \mu_{sg} - \epsilon$), (iii) *antagonistic* if one organism could grow faster while the other organism had a reduced growth rate, (iv) *commensal* if one species could grow faster in a pair and one did not show an altered growth rate ($\mu_{sg} + \epsilon > \mu_{cg} > \mu_{sg} - \epsilon$), (v) *amensal* if one organism had a reduced growth rate and the other organism's growth remained unchanged, and (vi) *neutral* if both species showed no difference between single- and co-growth rate. An ϵ of 10^{-6} was used to account for minor differences between predicted single- and co-growth rates that might occur due to unstable floating-point computations during linear optimization. In this study, we focused on mutualistic, competitive, and antagonistic interactions because only less than 1% (median) of the species pairs per sample were predicted to be commensal, amensal or neutral. All scripts for single- and co-growth simulations were implemented in R and are available at https://github.com/jotech/agora_interactions. To map 16S sequencing reads from each sample to the corresponding bacterial models from the AGORA resource and their predicted interactions, sequence reads were aligned against the 16S ribosomal rRNA gene sequences of the corresponding bacteria using USEARCH¹¹. Each sequence was mapped to the AGORA organism with the highest V4 16S sequence identity and sequence reads with less than 97% sequence identity were considered as bacteria that are not included in the AGORA collection. Next, we mapped for each sample the relative phylotype frequencies to every pair of AGORA organisms to calculate the relative pair abundance $c_{i,i} = c_i^2$ and $c_{i,j} = 2 * c_i \cdot c_j$, for $i \neq j$ where c_i and c_j are the relative abundances of the individual phylotypes i and j , respectively.

Prediction of metabolic interchange within bacterial communities

To assess metabolic activity of the microbial communities for each sample, the metabolic models of bacteria mentioned above were joined into a community simulation as described previously^{8,10}. Only bacterial species, which were detected with a relative abundance above 0.1% were included in the community model. To account for individual abundances, a 'community biomass reaction' was introduced that incorporated the biomass reactions of the individual bacteria in accordance with their relative abundances. Fluxes were determined using parsimonious flux balance analysis¹², by maximizing the production of community biomass subject to the above mentioned dietary constraints and concomitantly minimizing the total sum of fluxes (scaled with a factor of 10^{-5} in the objective function). For each case, optimality of the resulting objective function value was verified by maximizing biomass production without minimization of the total sum of fluxes. To accelerate computation dietary constraints were scaled by a factor of ten. For individual bacteria, active reactions were determined based on a threshold flux of 10^{-6} mmol/gDW/hr. To predict the activity of specific reactions on the community level all fluxes of the same biochemical reactions across all community members were summed and a threshold flux of 10^{-4} mmol/gDW/hr was used to decide which reactions are likely to be active and which are not- or only marginally utilized. For the two cohorts we

tested for significantly different predicted reaction activities between male and female samples within the healthy or IBD cohorts (pre-treatment) but did not observe significant differences.

Impact of different assumptions for dietary conditions

As mentioned above, the flux balance simulations for bacterial community metabolism requires the definition of the nutritional environment. Chemical composition of the environment of gut-inhabiting bacteria is decisively determined by the dietary habits of the human host¹³. Thus, also the model prediction might be strongly influenced by the nutritional assumptions for *in silico* simulations. Since all patients and healthy persons who were part of this study were located in northern Germany we assumed a standardized western diet as defined previously⁸. Nonetheless, for sake of completeness we compared the model predictions on the frequency on antagonistic, mutualistic, and resource competitive interactions also to a fictive diet high in fibres, such as arabinogalactan and xylan⁸ (Fig S11). For healthy controls, the models predict less antagonistic and competitive interactions compared to the western diets (see Fig. 3A). In contrast to western diet, levels of antagonistic interactions in IBD and RD did not significantly differ to healthy controls, but resource competitive interactions were still significantly more frequent in both disease entities if a high-fibre diet is used for model simulations. Thus, changing the dietary conditions had some impact on model predictions, but model simulations do not contradict the central observation of more abundant community-destabilizing competitive interactions during disease. Moreover, assuming a western diet is more accurate for the specific two cohorts used in this study.

Manual and literature-based corrections to AGORA metabolic models

While *in silico* simulating the metabolic processes within bacterial communities, we came across a number of inconsistencies in the original models (Version 1.01) that caused unrealistically high predicted flux rates for metabolic cross-feeding interactions (i.e. $> 500 \text{ mmol}\cdot\text{h}^{-1}\cdot\text{gDW}^{-1}$; in comparison, the maximum inflow flux of water is set to $10 \text{ mmol}\cdot\text{h}^{-1}\cdot\text{gDW}^{-1}$). These high fluxes were caused by futile cycles that involved the cyclic release and uptake of metabolites as depicted in the scheme shown in Figure S7. The corrections listed in Supplementary Table S6 prevented such cycles and include amendments in reaction stoichiometry and reversibility.

Statistical analysis of metabolomic data

Metabolites were analyzed from stool samples of 9 IBD subjects, treated with anti-TNF α antibody, which resulted in 4 non-remission and 5 remission patients at week 14. An orthogonal partial least squares discriminant analysis (OPLS-DA) was applied to find variables, responsible for the separation of remission and non-remission patients prior and after the treatment.

The robustness of the build model was verified by calculation of p-values with cross-validation analysis of variance (CV-ANOVA). The goodness of fit $R^2Y(\text{cum})$, the goodness of prediction $Q^2(\text{cum})$, and the p-values were reported as indicators for the significance of the models. The coefficients of regression of the models were considered in order to detect which metabolites are highly correlated (positively or negatively) with the different classes. All the classification models were done in SIMCA 13.0.3.0 (Umetrics, Umeå, Sweden), the box plots in RStudio (Version 1.0.136 – © 2009-2016, RStudio, Inc.) and the Mann-Whitney Rank Sum Test in SigmaPlot 12.0 (Systat Software Inc., San Jose, CA, USA).

Non-targeted metabolomics using HILIC-LC-MS/MS

Around 50 mg of fecal stool sample was weighed in sterile ceramic bead tubes (NucleoSpin® Bead Tubes, Macherey-Nagel, Dueren, Germany). One millilitre of pre-chilled (-20°C) methanol (LiChrosolv®, hypergrade for LC-MS, Merck KGaA, Darmstadt, Germany) was added to the stool sample and homogenized with Precellys® Evolution Homogenizer (Bertin Corp., Rockville, Maryland, United States of America; 4,500 rpm, $40\times 3 \text{ s}$, 2 s pause time). Samples were then centrifuged for 10 minutes at $21.000\times g$, cooled at 4°C . An aliquot of $100 \mu\text{L}$ was evaporated at 40°C (Savant, SPD121P, SpeedVac Concentrator, ThermoFisher Scientific, Waltham, Massachusetts, United States of America) and reconstituted with 75% acetonitrile (LiChrosolv®, hypergrade for LC-MS, Merck KGaA, Darmstadt, Germany) to perform hydrophilic interaction liquid chromatography (HILIC) coupled to mass spectrometry (MS) analyses. The robustness of the build model was verified

by calculation of p-values through the analysis of variance of the cross-validated predictive residuals (CV-ANOVA). In order to exclude possible overfitting, the significant level of p-value was set to 0.05.

Fecal samples and standard mixtures of 50 metabolites were analyzed on a time of flight mass spectrometer (maXis, Bruker Daltonics, Bremen, Germany), coupled to an UHPLC system (Acquity, Waters, Eschborn, Germany). A charge modulated hydroxyethyl Amide HILIC column (iHILIC®-Fusion UHPLC Column, SS, 100x2.1mm, 1.8 μ m, 100Å, (HILICON AB, Umea, Sweden)) was used to separate polar metabolites of stool samples. A stock solution of 0.5 molar ammonium acetate (Merck KGaA, Darmstadt, Germany) was adjusted to pH 4.6 with glacial acetic acid (Biosolve, Valkenswaard, Netherlands). MilliQH₂O was derived from Milli-Q Integral Water Purification System (Billerica, MA, United States of America). Mobile phase for HILIC separation consisted of 5 millimolar ammonium acetate in 95% acetonitrile, pH 4.6 (A) and 25 millimolar ammonium acetate in 30% acetonitrile, pH 4.6 (B). Elution of metabolites was performed with a flow rate of 0.5 mL/minutes, using a 0.1–99.9% phase B gradient over 7.5 minutes. At the start, 0.1% B was kept for 2 minutes with increasing step to 99.9%B within 7.5 minutes. 99.9%B was constant for 2.5 minutes with fast decrease to 0.1%B within 0.1 minutes and a pre-run time of 2.5 minutes at 0.1% B. The column oven temperature was set to 40 °C and the injection volume at partial loop was 5 μ L.

Mass spectrometry conditions

Internal calibration of mass spectrometer was done by injecting ESI-L Low Concentration Tuning Mix (Agilent, Santa Clara, CA, United States of America). External Calibration of mass spectrometer was ensured by injecting ESI-L Low Concentration Tuning Mix (1:4 diluted in 75% acetonitrile) in the first 0.3 minutes of each LC-MS run, introduced by a switching valve.

Mass spectra were acquired in positive and negative ionization mode (+/-ESI). ESI parameters were as follows: nitrogen flow rate of 10 L/minute, dry heater of 200°C, nebulizer pressure of 2.0 bar and capillary voltage of 4500V. Data was acquired in line and profile mode with acquisition rate of 5 Hertz. Data dependent MS/MS experiments were performed for each sample by fragmenting the three most intense ions within one scan (>2000 counts, active exclusion of 3 spectra, release after 0.1 minutes and reconsider precursor if current intensity/previous intensity \times 3). Collision energy was set to 10eV and isolation width of 8 Dalton.

Data processing

Raw LC-MS data were processed with Genedata Refiner MS software (Genedata GmbH, Munich, Germany), including chemical noise subtraction, calibration, chromatographic peak picking, deisotoping and metabolite library search (HMDB for MS1 level (\pm 0.005 Dalton))¹⁴ and spectral libraries derived from MasBank of North America (<http://mona.fiehnlab.ucdavis.edu>) including MassBank¹⁵, GNPS¹⁶, HMDB and LipidBlast¹⁷ for MS2 level (0.1 Dalton)). Final data matrix consisted of mass signals (m/z) and their respective retention time (RT) in minutes, called cluster with observed maximum intensity for each sample. Clusters with RT<1 minute were excluded from further analysis. Data was normalized to the wet sample weight and scaled (unit-variance) prior statistical analysis.

Supplementary References

- 1 Caporaso, J. G. *et al.* Ultra-high-throughput microbial community analysis on the Illumina HiSeq and MiSeq platforms. *The ISME Journal* **6**, 1621, doi:10.1038/ismej.2012.8 (2012).
- 2 Sul, W. J. *et al.* Bacterial community comparisons by taxonomy-supervised analysis independent of sequence alignment and clustering. **108**, 14637-14642, doi:10.1073/pnas.1111435108 %J Proceedings of the National Academy of Sciences (2011).
- 3 Guss, A. M. *et al.* Phylogenetic and metabolic diversity of bacteria associated with cystic fibrosis. *The ISME Journal* **5**, 20, doi:10.1038/ismej.2010.88 (2010).
- 4 Bradley, I. M., Pinto, A. J. & Guest, J. S. Design and Evaluation of Illumina MiSeq-Compatible, 18S rRNA Gene-Specific Primers for Improved Characterization of Mixed Phototrophic Communities. **82**, 5878-5891, doi:10.1128/AEM.01630-16 %J Applied and Environmental Microbiology (2016).
- 5 Al-hebshi, N. N. *et al.* Inflammatory bacteriome featuring *Fusobacterium nucleatum* and *Pseudomonas aeruginosa* identified in association with oral squamous cell carcinoma. *Scientific Reports* **7**, 1834, doi:10.1038/s41598-017-02079-3 (2017).
- 6 Orth, J. D., Thiele, I. & Palsson, B. Ø. What is flux balance analysis? *Nature Biotechnology* **28**, 245, doi:10.1038/nbt.1614 (2010).
- 7 Gudmundsson, S. & Thiele, I. Computationally efficient flux variability analysis. *BMC Bioinformatics* **11**, doi:10.1186/1471-2105-11-489 (2010).
- 8 Magnusdottir, S. *et al.* Generation of genome-scale metabolic reconstructions for 773 members of the human gut microbiota. *Nat Biotech* **35**, 81-89, doi:10.1038/nbt.3703 (2017).
- 9 Savinell, J. & Palsson, B. Network analysis of intermediary metabolism using linear optimization. I. Development of mathematical formalism. *J Theor Biol* **154**, 421-454 (1992).
- 10 Heinken, A., Sahoo, S., Fleming, R. M. T. & Thiele, I. Systems-level characterization of a host-microbe metabolic symbiosis in the mammalian gut. *Gut Microbes* **4**, 28-40, doi:10.4161/gmic.22370 (2013).
- 11 Edgar, R. C. Search and clustering orders of magnitude faster than BLAST. *Bioinformatics* **26**, 2460-2461, doi:10.1093/bioinformatics/btq461 (2010).
- 12 Lewis, N. E. *et al.* Omic data from evolved *E. coli* are consistent with computed optimal growth from genome-scale models. *Molecular Systems Biology* **6**, doi:10.1038/msb.2010.47 (2010).
- 13 Kau, A. L., Ahern, P. P., Griffin, N. W., Goodman, A. L. & Gordon, J. I. Human nutrition, the gut microbiome and the immune system. *Nature* **474**, 327, doi:10.1038/nature10213 (2011).
- 14 Wishart, D. S. *et al.* HMDB 4.0: the human metabolome database for 2018. *Nucleic Acids Research* **46**, D608-D617, doi:10.1093/nar/gkx1089 (2018).
- 15 Hisayuki, H. *et al.* MassBank: a public repository for sharing mass spectral data for life sciences. *Journal of Mass Spectrometry* **45**, 703-714, doi:10.1002/jms.1777 (2010).
- 16 Wang, M. *et al.* Sharing and community curation of mass spectrometry data with Global Natural Products Social Molecular Networking. *Nature Biotechnology* **34**, 828, doi:10.1038/nbt.3597 (2016).
- 17 Kind, T. *et al.* LipidBlast in silico tandem mass spectrometry database for lipid identification. *Nature Methods* **10**, 755, doi:10.1038/nmeth.2551 (2013).